Original Article

MOLECULAR METABOLISM

Liver matrin-3 protects mice against hepatic steatosis and stress response via constitutive androstane receptor

Xiao Cheng[1], Vijaya Bhaskar Baki[1], Matthew Moran[1], Baolong Liu[2], Jiujiu Yu[2], Miaoyun Zhao[3], Qingsheng Li[3], Jean-Jack Riethoven[4,5], Channabasavaiah B. Gurumurth[6], Edward N. Harris[1,5,7], Xinghui Sun[1,5,7,*]

ABSTRACT

Objective: The prevalence of metabolic dysfunction-associated steatotic liver disease (MASLD) continues to rise with the increasing obesity epidemic. Rezdiffra as an activator of a thyroid hormone receptor-beta is the only Food and Drug Administration approved therapy. As such, there is a critical need to improve our understanding of gene expression regulation and signaling transduction in MASLD to develop new therapies. Matrin-3 is a DNA- and RNA-binding protein involved in the pathogenesis of human diseases. Here we examined its previously uncharacterized role in limiting hepatic steatosis and stress response via the constitutive androstane receptor (CAR).

Methods: Matrin-3 floxed and liver-specific knockout mice were fed either a chow diet or 60 kcal% high-fat diet (HFD) for up to 16 weeks. The mice were euthanized for different analysis including liver histology, lipid levels, and gene expression. Bulk RNA-seq, bulk ATAC-seq, and single-nucleus Multiome were used to examine changes of transcriptome and chromatin accessibility in the liver. Integrative bioinformatics analysis of our data and publicly available datasets and different biochemical assays were performed to identify underlying the molecular mechanisms mediating matrin-3's effects. Liver-tropic adeno-associated virus was used to restore the expression of CAR for lipid, acute phase genes, and histological analysis.

Results: Matrin-3 expression is induced in the steatotic livers of mice. Liver-specific matrin-3 deletion exacerbated HFD-induced steatosis, acute phase response, and inflammation in the liver of female mice. The transcriptome and chromatin accessibility were re-programmed in the liver of these mice with signatures indicating that CAR signaling is dysregulated. Mechanistically, matrin-3 interacts with CAR mRNA, and matrin-3 deficiency promotes CAR mRNA degradation. Consequently, matrin-3 deletion impaired CAR signaling by reducing CAR expression. Matrin-3 levels positively correlate with CAR expression in human livers. Ces2a and Il1r1 were identified as new target genes of CAR. Interestingly, we found that CAR discords with the expression of its target genes including Cyp2b10 and Ces2a in response to HFD, indicating CAR signaling is dysregulated by HFD despite increased CAR expression. Dysregulated CAR signaling upon matrin-3 deficiency reduced Ces2a and de-repressed Il1r1 expression. CAR restoration partially abrogated the dysregulated gene expression, exacerbated hepatic steatosis, acute phase response, and inflammation in liver-specific matrin-3 knockout mice fed a HFD.

Conclusions: Our findings demonstrate that matrin-3 is a key upstream regulator maintaining CAR signaling upon metabolic stress, and the matrin-3-CAR axis limits hepatic steatosis and stress response signaling that may give insights for therapeutic intervention.

Keywords Matrin-3; Constitutive androstane receptor; Steatosis; Stress response; Signaling; Gene expression

1. INTRODUCTION

The prevalence of metabolic dysfunction-associated steatotic liver disease (MASLD) [1] continues to rise with the increasing obesity epidemic [2]. Rezdiffra is the only Food and Drug Administration (FDA) approved therapy and works as an activator of a thyroid hormone receptor-beta which partially decreases steatosis [3]. As such, there is a critical need to improve our understanding of gene expression regulation and signaling transduction in MASLD to develop new therapies. Matrin-3 is a DNA- and RNA-binding protein involved in the pathogenesis of human diseases [4–7]. For example, its mutation causes amyotrophic lateral sclerosis in humans [4]. Interestingly, 76% of patients with amyotrophic lateral sclerosis have hepatic steatosis [8,9]. As a nuclear matrix protein, matrin-3 plays important roles in regulating transcription factor activity [10], chromatin organization [11,12], RNA splicing [13,14], RNA modification [15], and RNA stability

[1]Department of Biochemistry, University of Nebraska — Lincoln, Beadle Center, 1901 Vine St, Lincoln, NE 68588, USA [2]Department of Nutrition and Health Sciences, University of Nebraska — Lincoln, 230 Filley Hall, Lincoln, NE 68583-0922, USA [3]Nebraska Center for Virology, School of Biological Sciences, University of Nebraska — Lincoln, Lincoln, NE, USA [4]Nebraska Center for Biotechnology, University of Nebraska — Lincoln, Beadle Center, 1901 Vine St, Lincoln, NE 68588, USA [5]Nebraska Center for Integrated Biomolecular Communication (NCIBC), University of Nebraska — Lincoln, Lincoln, NE 68588, USA [6]Mouse Genome Engineering Core Facility, University of Nebraska Medical Center, Omaha, USA [7]Nebraska Center for the Prevention of Obesity Diseases through Dietary Molecules, University of Nebraska — Lincoln, USA

*Corresponding author. Department of Biochemistry, University of Nebraska — Lincoln, Beadle Center, 1901 Vine St, Lincoln, NE 68588, USA. E-mail: xsun17@unl.edu (X. Sun).

Received March 7, 2024 • Revision received June 20, 2024 • Accepted June 21, 2024 • Available online 25 June 2024

https://doi.org/10.1016/j.molmet.2024.101977

Abbreviations

Acad11	acyl-CoA dehydrogenase family member 11
AHR	the aryl hydrocarbon receptor
ATAC-seq	the assay for transposase-accessible chromatin with sequencing
CAR	constitutive androstane receptor
ChIP	chromatin immuno-precipitation
DEGs	differentially expressed genes
EC	endothelial cells
FXR	the farnesoid X receptor
GFP	green fluorescent protein
Hep	hepatocytes
HFD	high-fat diet
HSC	hepatic stellate cells
IL1R1	interleukin 1 receptor type 1
IL10	interleukin 10
KC	Kupffer cells
Leuk	leukocytes
LXR	the liver X receptor
MASLD	metabolic dysfunction-associated steatotic liver disease
Matr3$^{fl/fl}$	floxed matrin-3 mice
Matr3 LKO	liver-specific matrin-3 knockout mice
PXR	the pregnane X receptor
RNA-seq	RNA sequencing
SAA1	serum amyloid A1
TBG	thyroxine-binding globulin

[16]. By doing so, matrin-3 is involved in cellular differentiation [10,12], mitotic spindle dynamics [13], cell survival [17], and the immune response [14,15]. However, the role of matrin-3 in metabolic disease remains completely unknown. We previously identified matrin-3 as a protein binding partner of maternally expressed gene 3, a long-noncoding RNA regulating the DNA damage response, preventing cellular senescence and obesity-induced insulin resistance [18,19]. We decided to study matrin-3 in MASLD because of its possible application to MASLD, a chronic syndrome that induces cellular senescence and insulin resistance.

Hepatic steatosis, a prominent characteristic of MASLD [20], is the accumulation of neutral lipids, typically triglycerides, in the liver resulting from an imbalance between lipid deposition and removal [20]. The constitutive androstane receptor (CAR) is a nuclear receptor family member initially identified as a xenobiotic nuclear receptor important in drug metabolism [21,22]. Later, it was recognized as a lipid sensor crucial in hepatic lipid homeostasis [23–25]. Metabolic and nutritional stress induce CAR expression in rodents [26,27]. Recently, nuclear CAR protein expression was found to correlate with steatohepatitis in humans [28]. CAR activation by its agonist TCPOBOP reduces the levels of hepatic triglycerides via different mechanisms in obese mice [24,25]. Global CAR knockout mice develop dyslipidemia and hepatic steatosis during aging [29] and display exacerbated hepatic steatosis and liver injury when fed a high-fat diet (HFD) [30]. The role of CAR in MASLD remains elusive regarding upstream mechanisms that control CAR signaling and the molecular basis by which CAR regulates hepatic steatosis.

The acute-phase response represents the initial response of an organism to restore tissue homeostasis and repair in response to infection and tissue damage [31]. In the process, hepatocytes undergo transcriptional reprogramming to produce and secrete different acute-phase proteins. When the acute-phase response becomes chronic, it may cause tissue damage [32]. For example, several acute-phase proteins such as serum amyloid A1 (SAA1) promote hepatic steatosis [33]. Nuclear receptors are important for gene expression in metabolism, immunity, and inflammation [34]. Recently, it was found that CAR is required for the expression of anti-inflammatory cytokine IL-10 in T cells indicating its role in the resolution of inflammation [35]. However, the role of CAR in hepatic acute-phase response remains elusive.

In this study, we uncovered new insights into the regulation of CAR signaling by matrin-3 and the regulation of hepatic steatosis and acute phase response by the matrin-3-CAR axis employing liver-specific matrin-3 knockout, multi-omics, and biochemical approaches. We found that matrin-3 interacts with CAR mRNA and matrin-3 deficiency promotes CAR mRNA degradation. Matrin-3 deletion leads to dysregulated CAR signaling by reducing CAR expression in the liver of mice and by changing the landscape of chromatin accessibility. Matrin-3 expression positively correlates with CAR expression in human livers, suggesting the regulation of CAR signaling in humans. We identified Ces2a and Il1r1 as new target genes of CAR signaling. We found that CAR is highly expressed in the nuclei of hepatocytes in mice. Dysregulated CAR signaling upon matrin-3 deficiency reduced Ces2a and de-repressed Il1r1 expression. CAR restoration partially abrogated the dysregulated gene expression, exacerbated hepatic steatosis, acute phase response, and inflammation in liver-specific matrin-3 knockout mice. Thus, matrin-3 is a key upstream regulator maintaining CAR signaling in response to metabolic stress, and the matrin-3-CAR axis limits hepatic steatosis, inflammation, and stress response signaling that might constitute a strategy for therapies.

2. RESULTS

2.1. Liver-specific matrin-3 deficiency exacerbates high-fat diet-induced hepatic steatosis

Matrin-3 is one of the nuclear-matrix-associated proteins [36]. In line with that, cytoplasmic and nuclear fractionation assay revealed that matrin-3 is indeed highly expressed in the nuclear fraction of mouse livers with low expression in the cytoplasmic fraction (Figure S1A). And its expression is not different at protein levels in the liver between male and female mice (Figure S1B). Immunostaining revealed that matrin-3 protein expression was increased 1.4-fold and 1.7-fold, respectively, in the livers of high-fat diet (HFD)-fed female and male mice compared with that in the livers of chow-fed female and male mice (Figure S1C, S1D), suggesting an adaptive or maladaptive role of matrin-3 in fatty liver disease. Interestingly, we found that matrin-3 expression was detected in a subset of hepatocytes in the liver, and the percentage of matrin-3-positive hepatocytes increased in both HFD-fed female and male mice (Figure S1C, S1E). To determine the role of matrin-3 in the liver, we generated matrin-3 conditional knockout mice (**Matr3$^{fl/fl}$**) by flanking exon 3 of the matrin-3 gene (Matr3) with loxP sites (Figure 1A and Figure S2). Matr3$^{fl/fl}$ mice were bred with Albumin-Cre mice to generate liver-specific matrin-3 knockout mice (Matr3$^{fl/fl}$;Alb-Cre+), hereafter called **Matr3 LKO** mice. Matr3 LKO mice were born at the expected Mendelian ratio and appeared grossly normal on a regular chow diet for at least one year. They gained similar body weight compared to Matr3$^{fl/fl}$ mice with a dramatic reduction of matrin-3 expression in the liver at 12 weeks of age (Figure S3A). Bulk RNA sequencing (RNA-seq) identified 646 (Padj $<$ 0.05) and 145 (Padj $<$ 0.05) differentially expressed genes (**DEGs**) in the livers of female and male mice, respectively, at 16 weeks of age (Figure S3B–

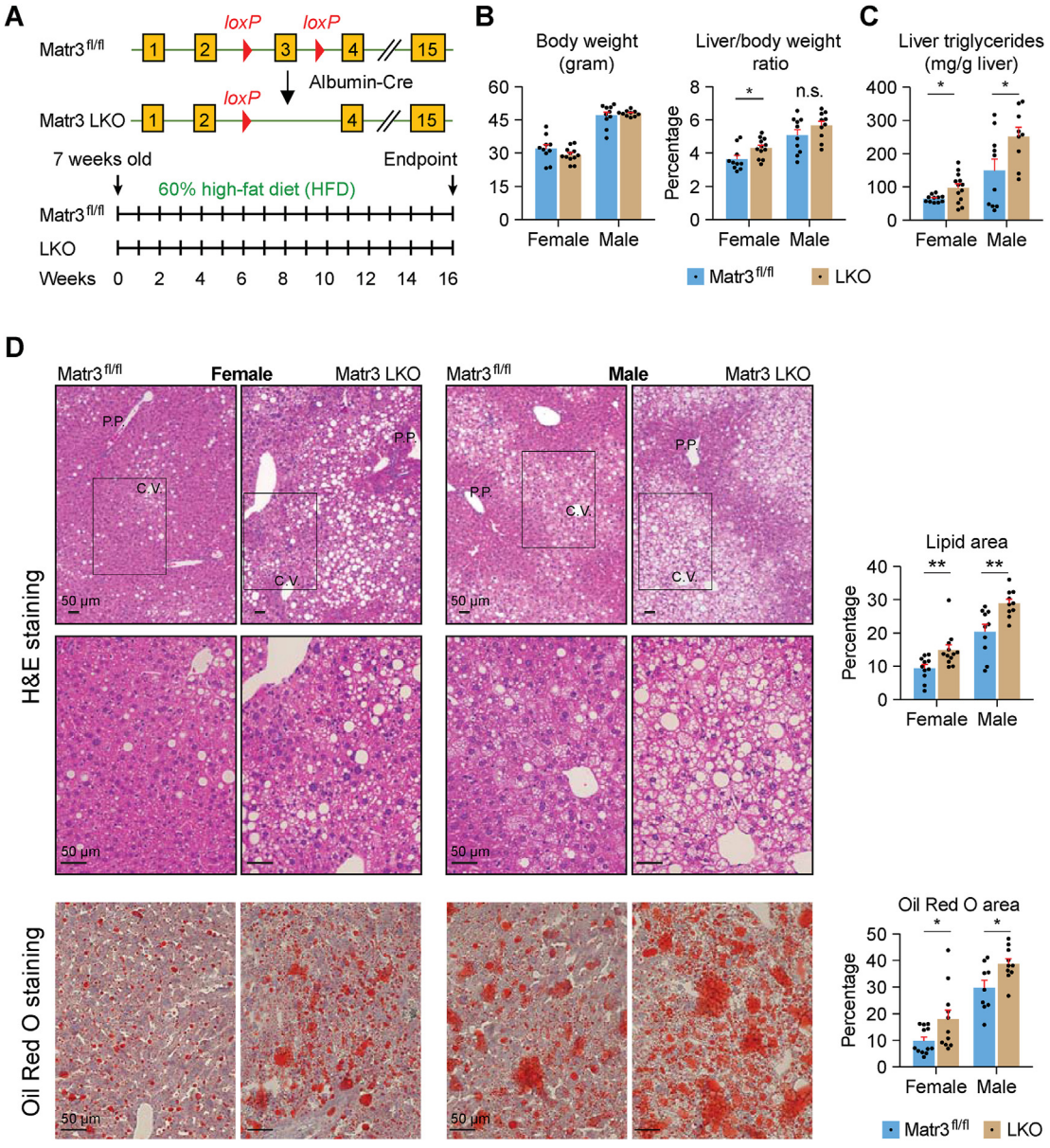

Figure 1: Liver-specific matrin-3 deficiency exacerbates high-fat diet-induced hepatic steatosis.
(A) Schematic of the generation of Matr3$^{fl/fl}$ and Matr3 LKO mice.
(B) Body weights in grams of Matr3$^{fl/fl}$ and Matr3 LKO mice, and liver/body weight ratios in percentage.
(C) The levels of liver triglycerides.
(D) Representative images of H&E staining and Oil Red O staining showing that matrin-3 deficiency aggravates hepatic steatosis. Lipid areas and Oil Red O-positive areas were quantified using ImageJ.
Mice were fed a 60 kcal% HFD for 16 weeks. Data are presented as mean ± SEM; n = 10–12 mice per group; $^{*}P < 0.05$, $^{**}P < 0.01$.

S3C; Table S2A). Enrichr analysis of these DEGs revealed several common Hallmark terms including cholesterol homeostasis, fatty acid metabolism, xenobiotic metabolism, and epithelial—mesenchymal transition between female and male mice (Figure S3B—S3C). We examined the levels of triglycerides in the liver of chow-diet-fed mice and did not observe any differences between Matr3$^{fl/fl}$ and Matr3 LKO mice (Figure S3D). After Matr3 LKO mice were fed a HFD for 16 weeks, western blot analysis revealed that matrin-3 protein was not detectable in the livers (Figure S3E). The glucose tolerance test and insulin tolerance test revealed that glucose homeostasis was not changed in Matr3 LKO mice (Figure S3F). There are no differences in body weights for either female or male mice between Matr3$^{fl/fl}$ and Matr3 LKO groups (Figure 1B), while female, not male, Matr3 LKO mice had an increased liver/body weight ratio after 16-week HFD (Figure 1B). Both female and male Matr3 LKO mice had higher levels of liver triglycerides (Figure 1C). Consistent with the data, Hematoxylin and Eosin (H&E) staining showed that the lipid areas are 1.5-fold and 1.4-fold higher in female and male Matr3 LKO mice than in female and male Matr3$^{fl/fl}$ mice, respectively (Figure 1D). The distribution of HFD-induced steatosis is predominant in the pericentral regions of the livers as previously reported [37], which is exacerbated in the livers of Matr3 LKO mice (Figure 1D). In addition, Oil Red O staining revealed that Oil Red

O-positive areas are 1.8- and 1.3-fold higher in female and male Matr3 LKO mice than in their respective control mice (Figure 1D).

To determine the potential mechanisms underlying lipid accumulation in the livers of Matr3 LKO mice, we examined triglyceride secretion and fatty acids uptake in the livers. Triglyceride secretion through very low-density lipoprotein particles is not different in the livers between Matr3$^{fl/fl}$ and Matr3 LKO mice (Figure S4A). It is interesting to note that Matr3 LKO livers have a reduced fatty acids uptake than Matr3$^{fl/fl}$ livers (Figure S4B), suggesting a feedback inhibition of fatty acids uptake due to a greater lipid accumulation in the livers of Matr3 LKO mice. The feedback inhibition of fatty acids uptake is sufficient to maintain fatty acid homeostasis in the livers of Matr3 LKO mice as the profile of 18 fatty acids is unaltered in the livers (Figure S4C). These results suggest that liver-specific deletion of matrin-3 exacerbates hepatic steatosis independent of triglyceride secretion and fatty acids uptake in the HFD-fed mice.

2.2. Liver-specific matrin-3 deficiency re-programs the hepatic transcriptome with gene signatures enriched for xenobiotic metabolism pathway, acute-phase and inflammatory response signaling

Consequently, we sought to characterize molecular pathways that contribute to the aggravated hepatic steatosis in Matr3 LKO mice and performed bulk RNA sequencing (RNA-seq) of the livers from HFD-fed Matr3$^{fl/fl}$ and Matr3 LKO mice of both sexes (n = 4 mice per group each sex). Quality control metrics for bulk RNA-seq data are shown in Table S2B. We identified 1333 and 239 DEGs [|log$_2$fold change| > log$_2$(1.5) & *P*adj < 0.05] in the livers of female and male Matr3 LKO mice, respectively (Figure 2A; Table S2C). Gene Set Enrichment Analysis revealed that the topmost downregulated Gene Ontology (**GO**) Biological Process was the "Xenobiotic metabolic process" (Figure 2B and C), while among the top upregulated GO biological processes were the "Acute inflammatory response" and "Acute

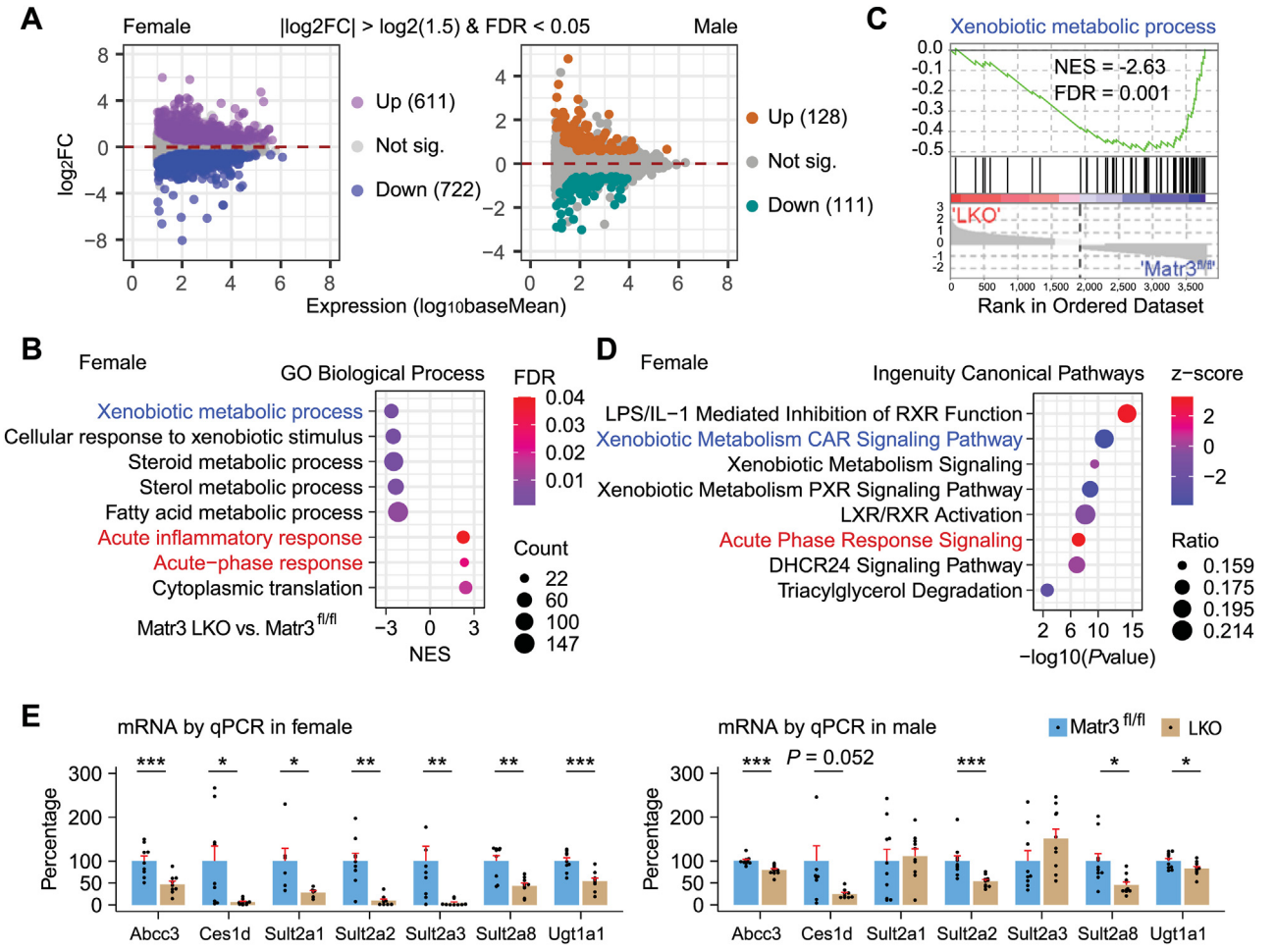

Figure 2: Liver-specific matrin-3 deficiency re-programs the hepatic transcriptome with gene signatures enriched for xenobiotic metabolism pathway, acute-phase and inflammatory response signaling.

(A) Bulk RNA-seq identified the differentially expressed genes (DEGs) in the livers of HFD-fed female and male mice (Matr3 LKO vs. Matr3$^{fl/fl}$), respectively. Mice were fed a 60 kcal % HFD for 16 weeks. The y-axis represents the log2 fold change, and the x-axis represents the log10 base mean from DEseq2. The base mean represents the average of the normalized count values taken over all samples.

(B) Gene Set Enrichment Analysis revealed top Gene Ontology Biological Process terms that are enriched in female Matr3$^{fl/fl}$ or Matr3 LKO mice.

(C) Enrichment plot of xenobiotic metabolic process.

(D) Top upregulated (red) or downregulated (blue) Ingenuity Canonical Pathways in the liver of female LKO mice.

(E) Real-time qPCR analysis of the indicated genes in the liver of female and male mice. Female mice, n = 9 per group for genes except Sult2a1 (n = 6 per group); male mice, n = 9–11 per group.

Bulk RNA-seq was performed with four mice per group. Data are presented as mean ± SEM. *$P < 0.05$, **$P < 0.01$, ***$P < 0.001$.

phase response" in the liver of female LKO mice (Figure 2B). In addition, Ingenuity Canonical Pathways including "Xenobiotic Metabolism CAR Signaling Pathway" and "Acute Phase Response Signaling" were downregulated and upregulated, respectively, in the liver of female LKO mice (Figure 2D). Several GO terms related to lipid metabolism and xenobiotic metabolism were enriched in the livers of male mice (Figure S5A—S5C). Real-time qPCR revealed that the expression of many genes involved in xenobiotic metabolism was reduced in the liver of female LKO mice and to a lesser extent in the liver of male LKO mice (Figure 2E). The liver is composed of several cell types. To examine the change in the transcriptome in hepatocytes, we performed single-nucleus Multiome on the livers of HFD-fed female Matr3$^{fl/fl}$ and Matr3 LKO mice. After quality control filtering and removal of putative doublets, single-nucleus RNA-seq clusters were assigned to five different cell types, including hepatocytes (Hep), Kupffer cells (KC), endothelial cells (EC), hepatic stellate cells (HSC), and leukocytes (Leuk) (Figure S5D). These cells have cell-type-specific expression of many genes, including Glul, Hnf4a, Nr1i3, Ppara in hepatocytes; Flt1, Pecam1, Kdr, Stab2 in endothelial cells; Ank3, Dcn, Reln, Rgs5 in hepatic stellate cells; Skap1, Trbc2, Ptprc in leukocytes; and Adgre1, Clec4f, and Slc8a1 in Kupffer cells (Figure S5D). Differential analysis of single-nucleus RNA-seq data identified 492, 231, and 203 DEGs (FDR $<$ 0.05 & fold change $>$ 1.5) using three different methods in the hepatocyte cluster between Matr3$^{fl/fl}$ and Matr3 LKO mice (Figure S5E; Table S2D). Enrichr analysis revealed that Hallmark terms such as "Oxidative phosphorylation", "Xenobiotic metabolism", "Bile acid metabolism", "Adipogenesis", and "Fatty acid metabolism" were enriched in hepatocytes (Figure S5F). Despite no terms relating to the acute phase response being enriched, the expression of several acute phase genes such as Hp, Hpx, Lcn2, Mt1, Mt2, Orm1, Orm2, Saa1, Saa2, and Saa3 was induced in the hepatocytes of Matr3 LKO mice (Table S2D). These bulk and single-nucleus RNA-seq data demonstrate that liver-specific matrin-3 deficiency re-programs the hepatic transcriptome with gene signatures mainly enriched for xenobiotic metabolism pathway, inflammation, and acute-phase response signaling.

2.3. Liver-specific matrin-3 knockout induces hepatic acute-phase response and inflammation in HFD-fed mice

The acute-phase response may cause tissue damage when it becomes chronic [32]. Gene Set Enrichment Analysis and Ingenuity Pathway Analysis of the bulk RNA-seq dataset revealed that acute phase response signaling is upregulated in the liver of female Matr3 LKO mice (Figure 2B and D). Indeed, the expression of many acute phase genes and inflammatory genes is increased in the liver of HFD-fed female but not male Matr3 LKO mice (Figure 3A and B). The production of these acute-phase proteins requires Stat3 activation [38,39]. Enrichr analysis of 611 upregulated DEGs in the liver of Matr3 LKO mice revealed that "IL-6/JAK/STAT3 signaling" is the most significantly enriched pathway (Figure 3C). In line with the analysis, the levels of phosphorylated Stat3 (Y705) were elevated by 3.8-fold (Figure 3D), indicating that Stat3 signaling is increased in the livers of HFD-fed female Matr3 LKO mice. Interestingly, we found that the expression of several acute phase genes including Apcs, Hp, and Orm2 was significantly increased in the liver of female but not male matrin-3 LKO mice fed a chow diet (Figure S6A). The levels of phospho-Stat3 tend to be increased in the liver of female matrin-3 LKO mice ($p = 0.058$) but not in male matrin-3 LKO mice fed a chow diet (Figure S6B). Consistent with the notion that female Matr3 LKO mice likely had increased hepatic inflammation compared with female Matr3$^{fl/fl}$ mice, the levels of liver and plasma IL-6 were elevated by 2.0-fold and 2.9-fold, respectively, while liver IL-1β levels were increased by 1.6-fold in HFD-fed female Matr3 LKO mice (Figure 3E). In addition, real-time qPCR revealed the mRNA expression of neutrophil markers including Ly6g, Elane, and Mpo was increased by 3.0-, 4.6-, and 5.7-fold, respectively, in the livers of HFD-fed female Matr3 LKO mice compared with Matr3$^{fl/fl}$ mice (Figure 3F). Myeloperoxidase (MPO) staining also revealed an increase in neutrophil infiltration (Figure 3F). Our data suggest that matrin-3 deficiency induces hepatic acute phase response signaling and inflammatory response in the liver of female Matr3 LKO mice.

2.4. Bulk ATAC-seq identified changes in chromatin accessibility in the livers of female Matr3 LKO mice

To delineate how changes in gene expression relate to genome-wide chromatin accessibility in the liver, we performed the assay for transposase-accessible chromatin with sequencing (ATAC-seq) (Figure 4A). The quality of ATAC-seq libraries was comparable between Matr3$^{fl/fl}$ and Matr3 LKO mice, as reflected by the similar TSS (transcription start site) enrichment scores (Figure S7A). Quality control metrics for ATAC-seq data are shown in Table S2B. In the liver of chow-fed mice, we identified 523 differential peaks among 88,203 peaks (FDR $<$ 0.05; 58 increased and 465 decreased) (Figure 4B; Table S2E). One hundred eighty-three genes proximal to these differential peaks were enriched for Hallmark terms such as "Xenobiotic Metabolism" by Enrichr (Figure 4C; Table S2E). TRRUST (Transcriptional Regulatory Relationships Unraveled by Sentence-based Text mining) database [40] analysis from Metascape [41] uncovered that Hnf4α is the main transcription factor regulating these peak-associated genes (Figure 4C). In the liver of HFD-fed mice, we identified 829 differential peaks (FDR $<$ 0.05; 525 increased and 304 decreased) among the total 105801 peaks (Figure 4D; Table S2F). Differential peaks that gained accessibility in Matr3 LKO livers were enriched in genomic regions 10—100 kb away from transcription start sites (Figure S7B, S7C). In comparison, differential peaks that lost accessibility are more likely located in regions within 1—10 kb downstream of the transcription start sites. These results suggest many genes had increased enhancer activity and a small percentage of genes had decreased direct promoter activity in the livers of female HFD-fed Matr3 LKO mice. Four hundred forty-four genes proximal to these differential peaks were enriched for Hallmark terms by Enrichr such as "Xenobiotic Metabolism" (Figure 4E; Table S2F). TRRUST database analysis from Metascape uncovered that Hnf4α and Nr1i3 (CAR) are the main transcription factors regulating these peak-associated genes (Figure 4E). These results demonstrate that matrin-3 deficiency alters the landscape of chromatin accessibility, and mainly affects chromatin accessibility at genomic loci of genes involved in xenobiotic metabolism in the livers of female Matr3 LKO mice. These results also indicate that CAR is the main transcription factor affected by matrin-3 deficiency in the liver of HFD-fed Matr3 LKO mice.

2.5. Matrin-3 LKO mice had dysregulated CAR signaling in the liver after 16 weeks of HFD feeding

We examined the expression of several nuclear receptors including Nr1i3 (encodes CAR) and others that are important in xenobiotic and lipid metabolism in the livers (Figure 5A). In female mice, matrin-3 liver-specific deletion reduced Nr1i3 expression by 61.0%, but not the expression of other nuclear receptors (Figure 5A). In male mice, matrin-3 LKO reduced the expression of Nr1i3, Nr1i2 (Pxr), Nr1h3 (Lxra), Nr1h4 (Fxr), and Ahr by 33.7%, 18.5%, 33.0%, 21.6%, and 26.4% respectively. However, matrin-3 LKO did not reduce the

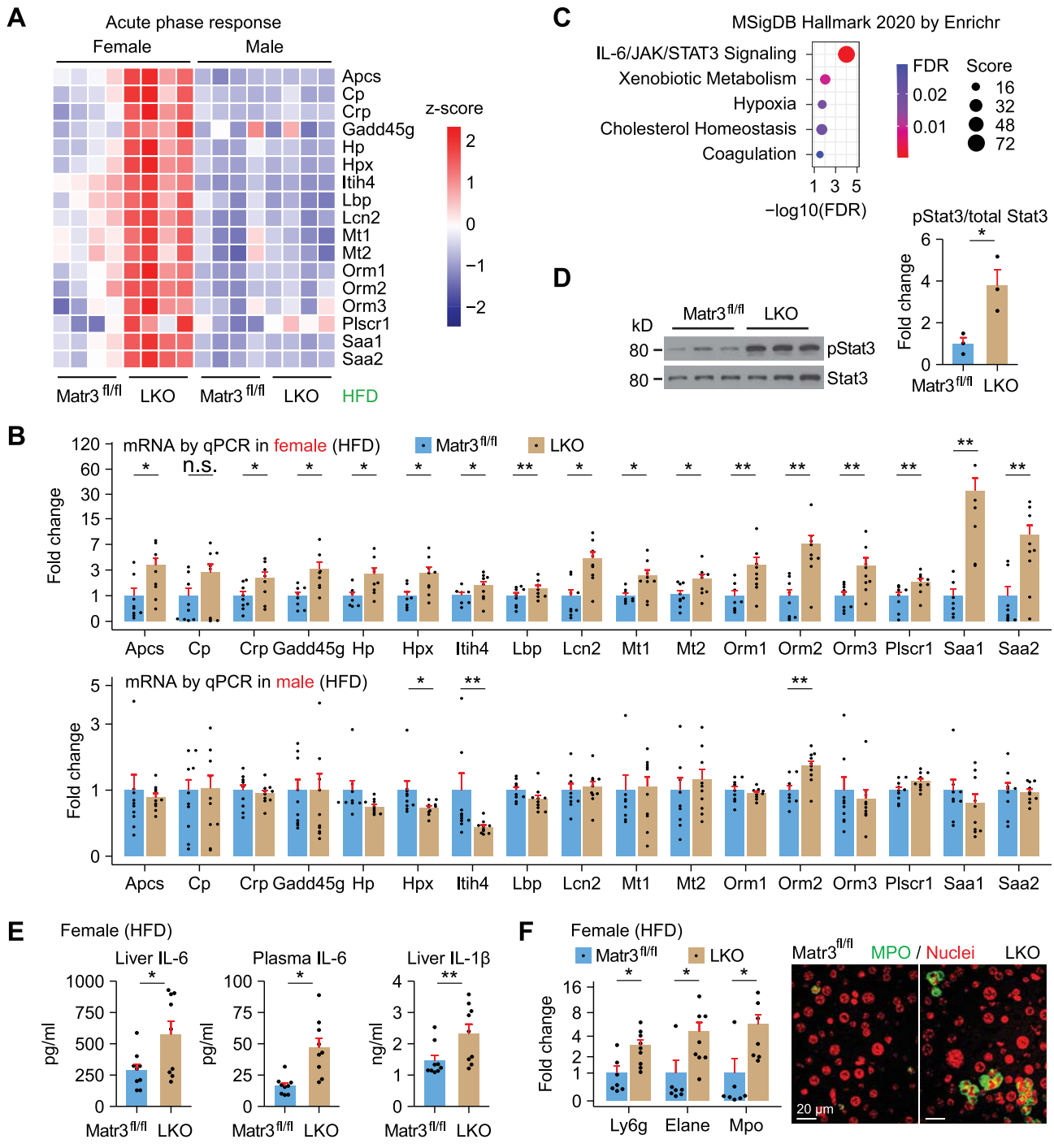

Figure 3: Liver-specific matrin-3 knockout induces the acute phase response and hepatic inflammation in the liver of HFD-fed mice.
(A) A heatmap shows the mRNA expression of genes involved in the acute-phase response and inflammation in the livers of female Matr3$^{fl/fl}$ and Matr3 LKO mice.
(B) Real-time qPCR analysis of genes involved in the acute-phase response and inflammation in the livers of Matr3$^{fl/fl}$ and Matr3 LKO mice (n = 8–9 mice per group).
(C) Top enriched Hallmark terms in the livers of female Matr3 LKO mice revealed by Enrichr analysis.
(D) Western blot analysis of pStat3 and total Stat3 in the livers of female Matr3$^{fl/fl}$ and Matr3 LKO mice (n = 3 per group).
(E) Levels of liver IL6, plasma IL6, and liver IL1β in the female Matr3$^{fl/fl}$ and Matr3 LKO mice detected by ELISA assays (n = 9 mice per group).
(F) Real-time qPCR analysis of neutrophil marker genes in the fatty livers of female Matr3$^{fl/fl}$ and Matr3 LKO mice (n = 7–9 mice per group). Immunostaining of the frozen sections of fatty livers was performed to stain myeloperoxidase (MPO) shown on the right. Nuclei are in red, and neutrophils are green.
Mice were fed a HFD for 16 weeks. Data are presented as mean ± SEM, $^{*}P < 0.05$, $^{**}P < 0.01$.

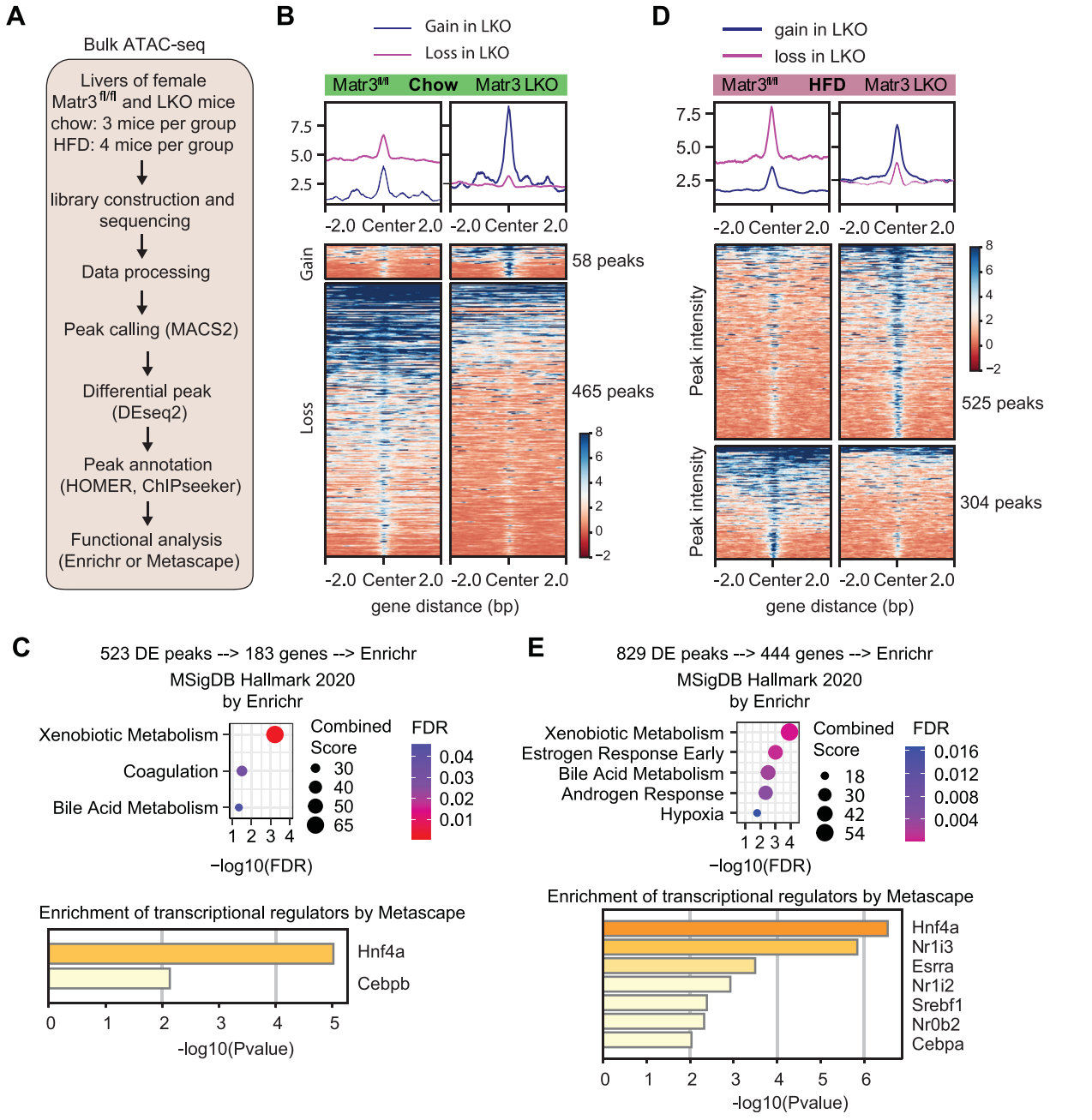

Figure 4: Bulk ATAC-seq identified changes in chromatin accessibility in the livers of female Matr3 LKO mice.
(A) Overview of ATAC-seq analysis. For mice fed a chow diet, 3 mice per group for six libraries; for mice fed a HFD, 4 mice per group for eight libraries.
(B) A heatmap shows the differential peaks in the livers between Matr3$^{fl/fl}$ and Matr3 LKO mice fed a chow diet.
(C) Enrichr and Metascape analysis of genes associated with the differential peaks in the liver of **chow**-fed mice revealed the enriched Hallmark terms and transcription factors, respectively.
(D) A heatmap shows the differential peaks in the livers between Matr3$^{fl/fl}$ and Matr3 LKO mice fed a HFD for 16 weeks.
(E) Enrichr and Metascape analysis of genes associated with the differential peaks in the liver of HFD-fed mice revealed the enriched Hallmark terms and transcription factors, respectively.

expression of the target genes of PXR (Egr1 and Gstm2) [42], LXR (Abcg5 and Abcg8) [43], FXR (Abcb4 and Shp) [44,45], and AHR (Tiparp) [46,47] (Figure S8A—S8D), while it reduced the expression of CAR target genes such as Cyp2b10, Cyp2c55 in the liver of HFD-fed or TCPOBOP-treated mice but not chow-diet-fed mice (Figure S8E, S8F, S8H). We found that matrin-3 LKO reduced the expression of Cyp3a11 (Figure S8A), a PXR target gene [48], while its expression was also induced by TCPOBOP (Figure S8G). Moreover, matrin-3 LKO reduced the expression of Cyp7a1 — an FXR target gene [45] (Figure S8C) and Cyp1a1 (Figure S8D) — an AHR target gene [49], suggesting matrin-3 deficiency also selectively regulates the expression of FXR and AHR target genes via unknown mechanisms. To examine CAR protein expression, we tested five commercial anti-CAR antibodies (Figure S9). The antibody from R&D systems (cat# PP-N4111-00) and the antibody

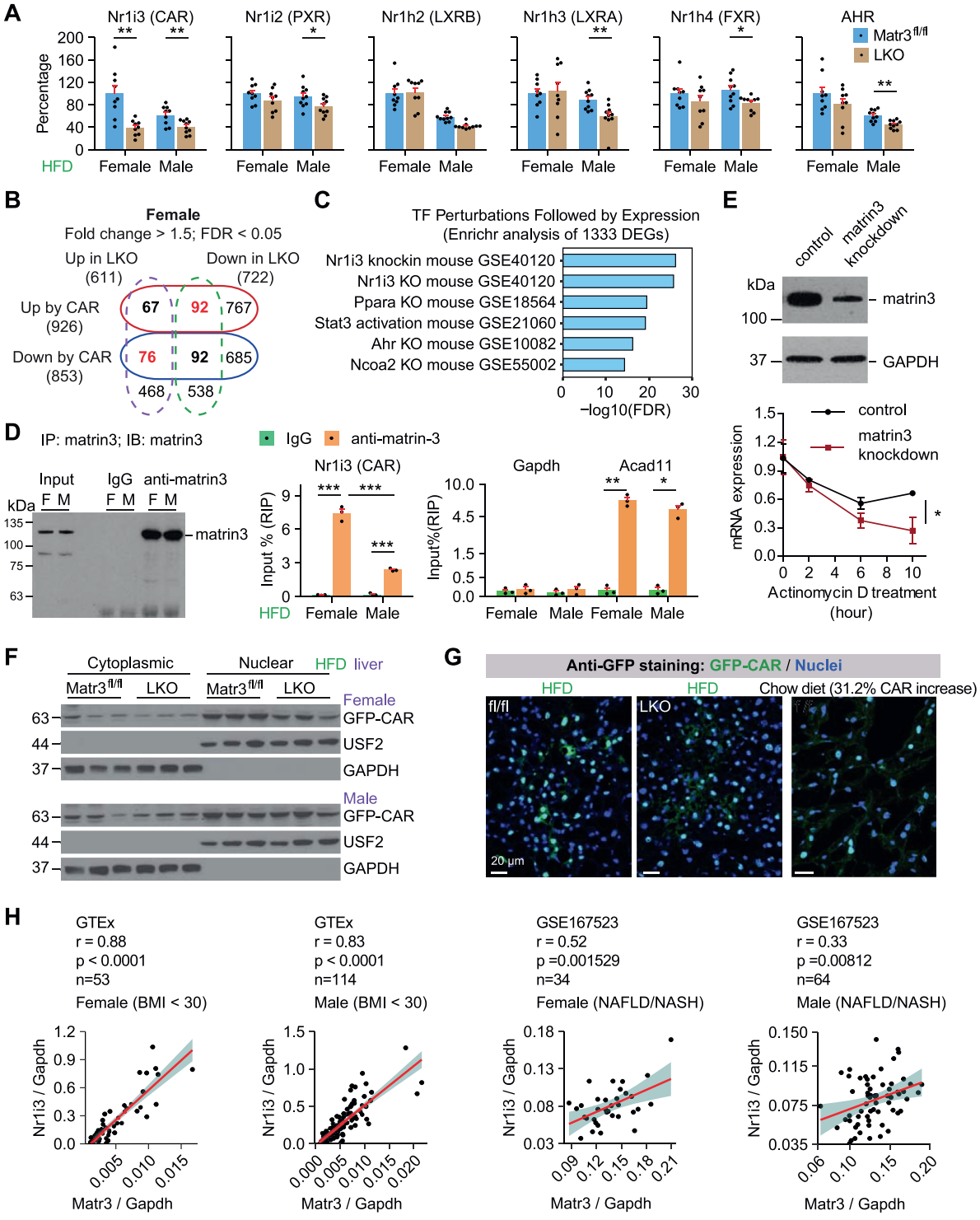

Figure 5: Matrin-3 LKO mice had dysregulated CAR signaling in the liver after 16 weeks of HFD feeding.

(A) Real-time qPCR analysis of the indicated genes in the livers of female or male mice fed a 60 kcal% HFD for 16 weeks (n = 8–10 mice/group).

(B) A Venn diagram shows the counter-regulated genes by CAR activation and matrin-3 liver-specific deficiency in the liver of female mice.

(C) Enrichr analysis of 1333 DEGs revealed transcription factor (TF) Perturbations Followed by Expression.

(D) RNA immunoprecipitation and real-time qPCR analysis reveal the interaction between matrin-3 and CAR mRNAs in the livers of female and male mice (n = 3 for each condition).

(E) Matrin-3 knockdown in mouse primary hepatocytes led to increased CAR mRNA degradation (n = 4 experiments).

(F) Western blot analysis of GFP-CAR (anti-GFP) in the cytoplasmic and nuclear fractions of the livers from Matr3$^{fl/fl}$ and Matr3 LKO mice.

(G) Liver sections were stained with anti-GFP antibodies to reveal GFP-CAR subcellular localization. The CAR mRNA levels were increased by 31.2% in the chow-diet-fed mouse injected with AAV8-TBG-GFP-CAR.

(H) Matrin-3 mRNA expression positively correlates with Nr1i3 (CAR) mRNA expression in human livers. Data are presented as mean ± SEM. $^{*}P < 0.05$, $^{**}P < 0.01$, $^{***}P < 0.001$.

from (LSBio cat# LS-C374482) can specifically detect mouse CAR when CAR is overexpressed. Both cannot detect endogenous CAR because they recognize another protein with a similar molecular weight as CAR but the signal is stronger (Figure S9). Our data suggest that matrin-3 deficiency dominantly reduced CAR mRNA expression not other nuclear receptors in the liver. To look further into the effects of matrin-3 on CAR signaling, we manually curated a list of 1779 CAR target genes compiled from three studies [42,50,51] (Table S2G) and examined the effects of matrin-3 LKO on the expression of CAR-regulated genes. Among 1333 DEGs regulated by matrin-3, 327 genes are regulated by CAR in female mice, while 168 genes are oppositely regulated by CAR (Figure 5B). Next, we did an Enrichr analysis of 1333 DEGs and identified transcription factors that likely control the expression of these DEGs (Figure 5C). The matrin-3-regulated transcriptome is represented by the changes in the transcriptome with gain-of- or loss-of-function of several transcription factors including CAR as the topmost candidate (Figure 5C). Matrin-3 is an RNA-binding protein [13,14] and matrin-3 deficiency reduces CAR mRNA (Figure 5A). This prompted us to examine matrin-3 and CAR mRNA interaction. RNA immunoprecipitation revealed that matrin-3 interacts with CAR mRNA in the livers of female and male mice (Figure 5D). Matrin-3 does not bind Gapdh mRNA [16], while it binds Acad11 mRNA as previously identified [13] (Figure 5D). Interestingly, the percentage of matrin-3-bound CAR mRNA is 3.1-fold higher in the livers of female mice than in male mice. Matrin-3 binds RNA molecules via its RNA-binding motifs [11,13,16,52,53] and the interaction stabilizes some of the RNA transcripts [16]. To examine whether matrin-3 regulates CAR mRNA stability, we measured CAR mRNA levels in mouse primary hepatocytes with or without matrin-3 silencing (Figure 5E). We found that matrin-3 knockdown in mouse primary hepatocytes promotes CAR mRNA degradation (Figure 5E). To reveal the role of matrin-3 on CAR translocation, we generated hepatotropic adeno-associated virus serotype 8 (AAV8) expressing GFP-tagged mouse CAR. GFP is at the N-terminus of CAR and does not affect CAR function [54—60]. GFP-CAR expression is driven by a liver-specific thyroxine-binding globulin (TBG) promoter. Eight-week-old $Matr3^{fl/fl}$ and LKO mice were injected with AAV8-TBG-GFP-mCAR (*i.v.* 1×10^{11} genome copies per mouse) to achieve physiological expression and fed a 60 kcal% HFD for 16 weeks. Cytoplasmic and nuclear fractionation assay and immunostaining followed by confocal imaging revealed that matrin-3 deficiency does not affect CAR nuclear translocation (Figure 5F and G). We surprisingly found that GFP-CAR is highly expressed in the nuclei of hepatocytes in the livers (Figure 5F and G). This was also observed in the liver of chow-diet-fed mice (Figure G). Lastly, we found that matrin-3 mRNA expression positively correlates with CAR mRNA expression in human livers, suggesting that matrin-3 likely also regulates CAR expression and signaling in the liver of humans (Figure 5H). Our data demonstrated that matrin-3 deficiency leads to dysregulated CAR signaling to a greater extent in the liver of female mice than in male mice.

2.6. Ces2a and Il1r1 are CAR direct target genes that are reduced and de-repressed, respectively, in the liver of Matr3 LKO mice

To identify CAR target genes that potentially mediate the aggravated steatosis and acute phase response in Matr3 LKO mice, we performed integrative analysis of matrin-3 and CAR oppositely regulated 168 genes (Figure 5B; Table S2H) for those that are associated with CAR ChIP-seq peaks from a previous study [54]. Among these 168 genes oppositely regulated by matrin-3 deficiency and CAR activation, 56 genes are associated with mouse CAR binding sites revealed by ChIP-seq in the liver of mice that were not treated with CAR agonist [54] (Figure 6A; Table S2I). We focused on Ces2a and Il1r1 because they are important in xenobiotic and lipid metabolism and acute phase response [61—66]. Ces2 has lipase activity [67] and decreased expression of Ces2 or Ces2a causes hepatic lipid accumulation [61,62]. Additionally, Ces2a deletion provokes severe hepatic steatosis and elevated inflammatory and fibrotic gene expression in mice fed a HFD [63]. If they are CAR direct target genes, their promoter regions must contain CAR binding sites, and their expression must be induced or repressed by CAR activation. First, we analyzed a published CAR ChIP-seq dataset [54], and the peaks of both human and mouse CAR are associated with the promoter regions of Ces2a and Il1r1 (Figure 6B and Figure S10), suggesting that they are CAR direct target genes. Importantly, our ChIP-qPCR data confirmed that mouse CAR binds to the genomic loci of Ces2a and Il1r1 in the liver (Figure 6C). Second, we found that short-term or long-term CAR agonist (TCPOBOP) treatment induced Ces2a and reduced Il1r1 expression in the liver (Figure 6D). These data demonstrated that Ces2a and Il1r1 are CAR direct target genes. The conclusion was also supported by previous studies showing that CAR activation induces Ces2a [68] and the promoter region of Il1r1 is associated with CAR binding sites revealed by ChIP-seq [35,54].

We next examined the expression of Ces2a and Il1r1 in the livers of Matr3 LKO and $Matr3^{fl/fl}$ mice. We found that Ces2a mRNA expression decreased in the livers of both female and male HFD-fed Matr3 LKO mice, while Il1r1 protein expression increased in the livers of female LKO mice with an increasing trend in the livers of male Matr3 LKO mice (Figure 6E). The results further support that CAR signaling is dysregulated in HFD-fed matrin-3 LKO mice. To deepen our understanding of Ces2a and Il1r1 regulation by CAR, we analyzed two published datasets from published studies [54,69] to examine whether the chromatin accessibility at CAR binding sites of Ces2a and Il1r1 genomic loci is changed by CAR activation. In one study [69], the authors examined chromatin accessibility in the liver of mice exposed to vehicle or TCPOBOP for either 3 h or 27 h. In another study, the authors identified genome-wide CAR binding sites in the liver of mice treated with or without CAR agonist TCPOBOP [54]. High levels of CAR are associated with both Ces2a and Il1r1 genomic loci in the absence of CAR agonist TCPOBOP which is not induced by TCPOBOP (Figure S10). The chromatin accessibility was increased by TCPOBOP at the CAR binding sites of the Ces2a genomic locus, while it was not changed at the Il1r1 genomic locus (Figure S10). We also examined chromatin accessibility at CAR binding sites of Ces2a and Il1r1 genomic loci in the liver of matrin-3 LKO mice (Figure S11). CAR ChIP-seq peaks are associated with both Ces2a and Il1r1 promoter regions in the absence of CAR agonist (Figure S11). Two ATAC-seq peaks indicated by red arrows are significantly increased at the Il1r1 genomic locus, while no significant ATAC-seq peaks were identified at the Ces2a genomic locus. These data demonstrate that the reduction of Ces2a expression in the liver of matrin-3 LKO mice is not associated with any changes in chromatin accessibility at Ces2a genomic locus, while the induction of Il1r1 is associated with increased chromatin accessibility adjacent to CAR binding sites at Il1r1 genomic locus.

To further investigate the regulation of CAR target genes by CAR signaling, we examined the expression of CAR and CAR target genes such as Ces2a and Cyp2b10 in the liver of mice. Interestingly, Ces2a expression was reduced in the liver of both male and female mice fed a HFD (Figure 6F), while CAR expression was induced (Figure 6F). The reduction of Ces2 was previously observed in diabetic *db*/*db* mice and HFD-fed mice [62]. Similarly, CAR target gene Cyp2b10 was also reduced by HFD in the liver of female mice (Figure S12A). Our data demonstrated that CAR expression discords on the expression of its

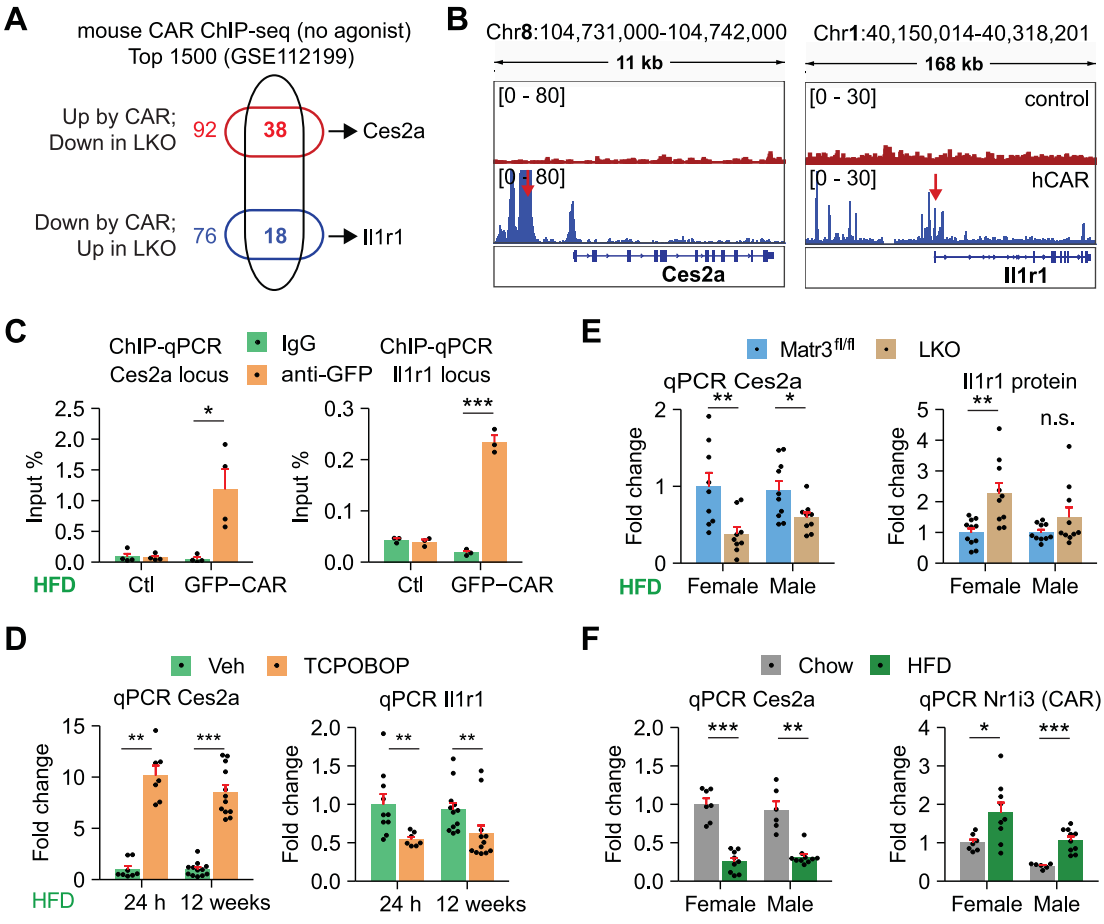

Figure 6: Ces2a and Il1r1 are CAR direct target genes that are reduced and induced, respectively, in the liver of Matr3 LKO mice.
(A) A Venn diagram shows 56 CAR direct target genes that are also regulated by matrin-3 in the liver.
(B) CAR binding sites revealed by ChIP-seq (GSE112199). Red arrows indicate the positions of ChIP-qPCR primers used in "C".
(C) ChIP-qPCR revealed that CAR binds to the genomic loci of Ces2a and Il1r1 (n = 3 or 4).
(D) Real-time qPCR analysis of Ces2a and Il1r1 in the livers of mice (n = 7–12 mice per group). Mice were treated with TCPOBOP at 3 mg/kg for 24 h or were weekly treated with TCPOBOP at 0.5 mg/kg (i.p.) for 12 weeks.
(E) Real-time qPCR analysis of Ces2a and western blot of Il1r1 in the livers of $Matr3^{fl/fl}$ and LKO mice (n = 8–10 mice per group) fed a HFD for 16 weeks.
(F) Real-time qPCR analysis of Ces2a and Nr1i3 (CAR) in the livers of mice fed a chow diet or 60 kcal% HFD for 16 weeks (n = 6–10 mice per group).
Data are presented as mean ± SEM, $*P < 0.05$, $**P < 0.01$, $***P < 0.001$.

target genes Ces2a and Cyp2b10, indicating that CAR signaling is impaired to turn on the expression of both genes in the liver of female mice when mice are fed a HFD. In support of this, we found that HFD selectively acts against CAR signaling on the expression of 218 (71 + 147) and 153 (62 + 91) genes in the livers of female and male mice, respectively (Figure S12B; Table S2J). Among these HFD and CAR inversely regulated genes, 64 (19 + 45) are common between female and male mice (Figure S12B). We then examined the correlation of CAR and its target genes in MASLD patients. The Pearson correlation coefficients between CAR and its-induced genes are higher in the livers of control subjects than in the livers of MASLD patients (Figure S12C), indicating that CAR is not as effective in inducing the expression of its target genes in human fatty livers as in lean livers. These data suggest that CAR signaling was dysregulated in fatty livers by unknown mechanisms such as CAR post-translational modifications, which potentially contribute to the dysregulated CAR signaling in Matr3 LKO mice.

In summary, we demonstrated that Ces2a and Il1r1 are CAR direct target genes; the reduction of Ces2a expression in the liver of matrin-3 LKO mice is not associated with any changes of chromatin accessibility at Ces2a genomic locus, while the induction of Il1r1 is associated increased chromatin accessibility adjacent to CAR binding sites at Il1r1 genomic locus; CAR expression discords on the expression of its target gene Ces2a and Cyp2b10 in the liver of mice fed a HFD, and Ces2a reduction in the liver of matrin-3 LKO mice involves the reduction of CAR expression and likely other unknown mechanisms such as CAR post-translational modifications due to HFD.

2.7. The restoration of CAR expression partially attenuates hepatic steatosis and stress response in female Matr3 LKO mice

Because we found that matrin-3 deficiency reduces CAR expression in the liver of mice fed a HFD, we reasoned that the restoration of CAR expression attenuates the phenotypes we observed in the livers of Matr3 LKO mice. $Matr3^{fl/fl}$ and Matr3 LKO mice were injected with AAV-TBG-GFP or AAV-TBG-GFP-CAR in week 9 on a 16-week HFD (Figure 7A). In $Matr3^{fl/fl}$ and Matr3 LKO mice received AAV8-TBG-GFP, CAR mRNA expression is 32.5% lower in the livers of Matr3 LKO mice than in $Matr3^{fl/fl}$ mice (Figure 7B). CAR mRNA expression was 3.6- and

3.2-fold higher, respectively, in Matr3$^{fl/fl}$ and Matr3 LKO mice that received AAV8-TBG-GFP-CAR than in Matr3$^{fl/fl}$ mice that received AAV8-TBG-GFP (Figure 7B). Immunostaining revealed that GFP-CAR was readily detected in the nuclei of both Matr3$^{fl/fl}$ and Matr3 LKO mice (Figure 7C). The restoration of CAR expression normalized the mRNA expression of Ces2a and Il1r1 that was significantly reduced and increased, respectively, in the livers of LKO mice than in Matr3$^{fl/fl}$ mice (Figure 7D). Next, we examined the effects of GFP-CAR expression on hepatic steatosis. We found that the levels of hepatic triglyceride are significantly higher in the livers of Matr3 LKO mice than in Matr3$^{fl/fl}$ mice that received AAV8-TBG-GFP, which was abrogated by the restoration of CAR expression (Figure 7E). The results were

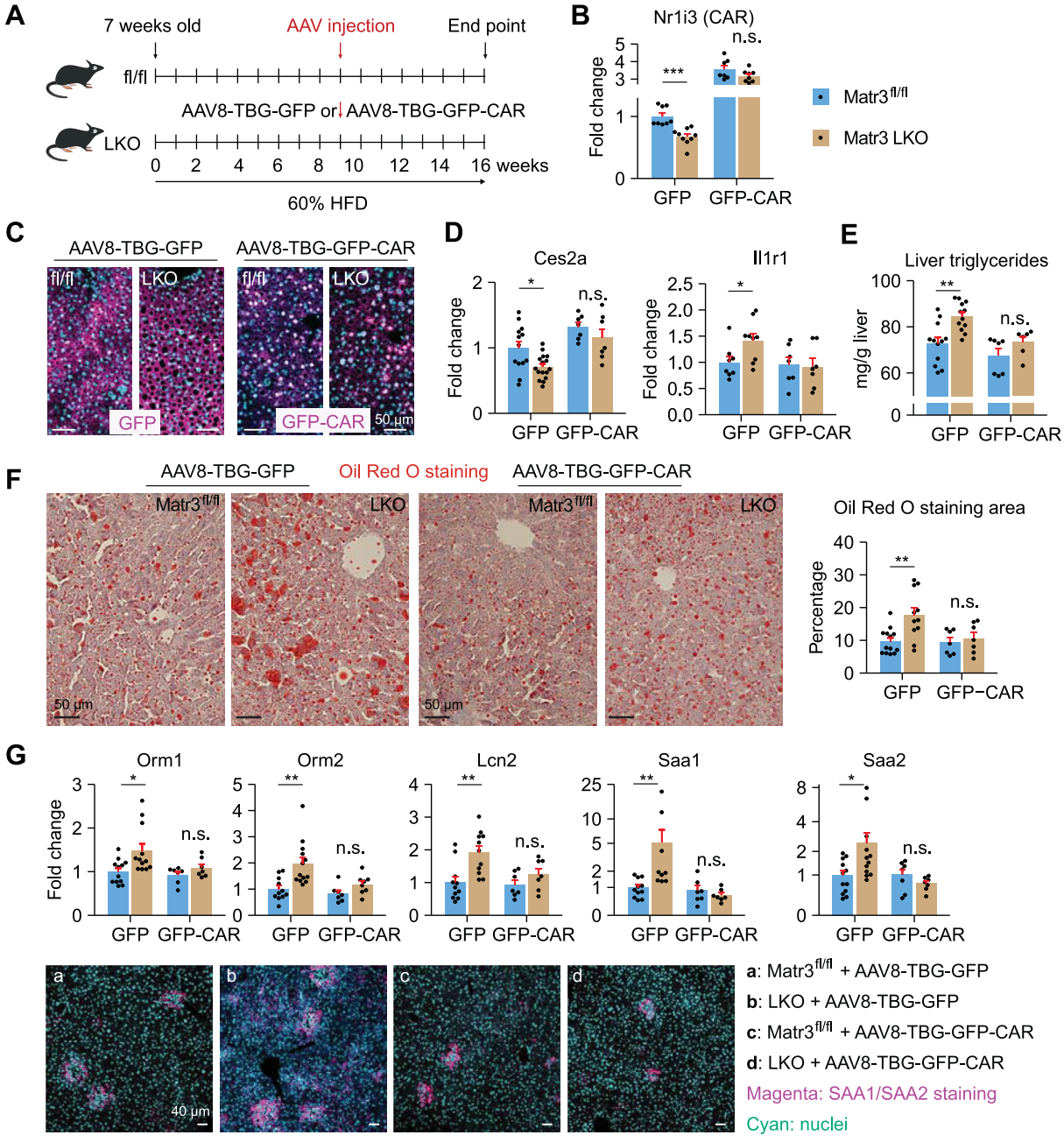

Figure 7: The restoration of CAR signaling partially attenuates hepatic steatosis and stress response in the liver of female Matr3 LKO mice.
(A) Schematic diagram of experimental timeline for AAV-TBG-GFP or AAV-TBG-GFP-CAR injection and 60 kcal% HFD in female Matr3$^{fl/fl}$ and Matr3 LKO mice.
(B) Real-time qPCR analysis of CAR mRNA expression in the livers of mice.
(C) Immunostaining of GFP or GFP-CAR in the livers of mice.
(D) Real-time qPCR analysis of Ces2a and Il1r1 mRNA expression in the livers of Matr3$^{fl/fl}$ and Matr3 LKO mice.
(E) The levels of hepatic triglyceride.
(F) Oil Red O staining of liver sections and quantification.
(G) Real-time qPCR analysis of genes involved in the acute-phase response and immunostaining of SAA1/SAA2 in the livers of Matr3$^{fl/fl}$ and Matr3 LKO mice. Nuclei are in cyan and SAA1/SAA2 are in magenta.
Data are presented as mean ± SEM, n = 7–16 per group; $^{*}P < 0.05$, $^{**}P < 0.01$.

consistent with Oil Red O staining of neutral lipids on liver frozen sections (Figure 7F). Lastly, the expression of Orm1, Orm2, Saa1, Saa2, and Lcn2 mRNAs was significantly higher in the livers of LKO mice than in Matr3$^{fl/fl}$ mice expressing GFP (Figure 7G), which was normalized by CAR restoration (Figure 7G). Immunostaining of SAA1/SAA2 confirmed that increased SAA1/SAA2 expression in the livers of Matr3 LKO mice was abrogated when GFP-CAR was expressed (Figure 7G). These results provide further evidence that matrin-3 deficiency causes dysregulated CAR signaling in the livers, which in turn promotes lipid accumulation and acute-phase response through CAR target genes. Our data indicate that CAR restoration can attenuate hepatic steatosis and immune-inflammatory response in MASLD.

3. DISCUSSION

In this study, we found that liver-specific matrin-3 deficiency exacerbates hepatic steatosis, inflammation, and acute phase response. Mechanistically, matrin-3 interacts with CAR mRNA, and matrin-3 deficiency promotes CAR mRNA degradation; liver-specific matrin-3 deficiency leads to dysregulated CAR signaling partially resulting from the reduced CAR expression and the changes of chromatin accessibility in the liver. As an upstream regulator of CAR signaling, matrin-3 deficiency altered the expression of CAR target genes including two direct target genes Ces2a and Il1r1 that we identified in the study. Lastly, CAR restoration normalizes the expression of CAR target genes, acute phase response genes, and ameliorates hepatic steatosis and inflammation. These new findings improve our understanding of the matrin-3-CAR axis in the etiology of MASLD.

CAR is a member of the nuclear receptor family. It has relatively high basal activity and is constitutively active displaying ligand-independent transcriptional activity [70,71]. The regulation of CAR activation is unique because of its intrinsic constitutive nature. The prevailing view is that CAR resides in the cytoplasm sequestered by cytosolic protein complexes [72]. The de-phosphorylation of CAR releases it from the cytosolic protein complexes allowing its translocation into the nucleus [73]. However, this prevailing view is challenged by a recent study showing that ectopic human CAR isoform 1 is constitutively localized in the nucleus and bound to chromatin in mouse primary hepatocytes [74]. We found that GFP-tagged CAR is enriched in nuclei in the livers of mice fed either a HFD or chow diet (Figure 5F). Although unlikely, we cannot rule out the possibility that the GFP tag could artificially lead to the nuclear localization of CAR. Nonetheless, the mode of action of CAR as a transcription factor warrants future studies.

Matr3 liver-specific deficiency likely leads to the dysregulated CAR signaling through different mechanisms. First, we found that matrin-3 is required for maintaining CAR signaling in the livers and matrin-3 deficiency promotes CAR mRNA degradation. Matrin-3 stabilizes CAR mRNA likely through its direct interaction with CAR mRNA or other mechanisms independently of the direct interaction. Surprisingly, a higher percentage of CAR mRNA interacts with matrin-3 in the livers of HFD-fed female mice than in HFD-fed male mice (Figure 5D). This could result from differential CAR mRNA modification such as N6-methyladenosine or differential matrin-3 post-translational modification such as acetylation between females and males. Because of the greater effects of matrin-3 on CAR mRNA expression in the liver of female mice, liver-specific matrin-3 deficiency greatly impairs CAR signaling in the liver of females and to a lesser extent in the liver of male mice (Figures 2B, 2E, S5A, and S5B). Second, matrin-3 can regulate the expression of CAR target genes through chromatin remodeling. It was reported that matrin-3 stabilizes chromatin loop—domain interactions and Yin Yang 1-mediated enhancer—promoter interactions during cell differentiation [12]. We also found that matrin-3 controls chromatin accessibility revealed by ATAC-seq in both chow diet-fed and HFD-fed mice (Figure 4). Many genes associated with the differential peaks are enriched for Hallmark terms such as xenobiotic metabolism and transcriptional regulators such as CAR. Lastly, we speculate that unknown mechanisms such as CAR post-translational modification (e.g. phosphorylation) are involved. CAR post-translational modification could be regulated by either HFD or matrin-3 expression which is important for CAR to induce or repress gene expression. This can explain our interesting observation that CAR expression discords on the expression of its target genes such as Ces2a and Cyp2b10 in the liver of HFD-fed mice, and explain that the restoration of CAR expression only partially normalizes the expression of Ces2a, Il1r1, and other acute phase response genes (Figure 7). While we demonstrated that matrin-3 is an important regulator of CAR signaling, we cannot completely exclude the possibility that matrin-3 regulates other nuclear receptor signaling that contributes to the observed phenotypes in Matr3 LKO mice, because CAR shares many target genes with other nuclear receptors [50]. In addition, matrin3 interacts with many RNA transcripts as described in previous studies [11,13,16,52,53]. Matrin-3 could affect other nuclear receptor signaling through its interaction with other RNA molecules.

We demonstrated that Ces2a is a new target gene of CAR. Matrin-3 deficiency impairs CAR signaling resulting in a 61.9% and 37.2% reduction of Ces2a expression, respectively, in the livers of female and male LKO Mice (Figure 6E). This can lead to increased levels of plasma and liver triglycerides, as Ces2a deletion causes hepatic steatosis [63]. Consistent with the result, CAR restoration partially rescues Ces2a expression and hepatic triglyceride levels (Figure 7D—F). We reason that the reduction of Ces2a partially contributes to exacerbated hepatic steatosis in both female and male Matr3 LKO mice. Our results are significant because decreasing triacylglycerides reduces cardiovascular risk [75].

The matrin-3-CAR axis limits hepatic immuno-inflammatory response. Nuclear receptors have various functions regulating metabolism, immunity, and inflammation [34,76]. For example, nuclear receptor NHR-42 is a negative regulator of innate immunity, while it also promotes lipid droplet mobilization [77]; the pregnane X receptor is involved in not only immune disorders and inflammatory responses [78] but also hepatic steatosis [79]; the liver X receptors promote fatty acid and triglyceride synthesis and inhibit inflammation [80,81]. Recently, it was found that CAR is required for the expression of anti-inflammatory cytokine IL-10 in T cells indicating its role in the resolution of inflammation [35]. However, the role of CAR in hepatic immuno-inflammatory responses was not previously characterized in MASLD. This report filled in the knowledge gap by revealing that CAR inactivation induces IL1R1/Stat3-mediated acute-phase response in the liver of HFD-fed mice. We identified Il1r1 as a direct target gene of CAR that is transcriptionally repressed by CAR activation (Figure 6D). Matrin-3 deficiency skews CAR signaling selectively altering the expression of a subset of CAR target genes including the de-suppression of IL1R1 expression. Increased IL1R1 and IL-1β expression results in the over-activation of stat3 signaling in the liver of female Matr3 LKO mice which potentially causes exacerbated hepatic inflammation and acute phase response. Interestingly, liver-specific matrin-3 deficiency activates acute-phase response signaling and acute inflammatory response in the liver of female mice but not male mice. This is likely because CAR signaling was slightly impaired in the liver of male mice. As shown in Figure 5A, CAR mRNA expression was reduced by 61.0% and 33.7%, respectively, in the liver of female and male LKO mice. The CAR protein concentration could be mildly reduced or unchanged in the

nuclei of hepatocytes in the liver of male LKO mice. In support of this speculation, we found that IL1R1 protein was increased by 2.3-fold in the liver of female LKO mice due to the impaired CAR signaling and the de-suppression of Il1r1 expression by CAR, while it was not increased in the liver of male LKO mice (Figure 6E). The genomic binding of transcription factors is a function of both binding site affinity and transcription factor concentration [82]. Because of that, we speculate that CAR binding at the Il1r1 genomic locus is unchanged in the liver of male LKO mice.

In conclusion, matrin-3 is a key upstream regulator maintaining CAR signaling upon metabolic stress, and the matrin-3-CAR axis limits hepatic steatosis, acute phase stress response signaling, and inflammation in MASLD. CAR signaling restoration may provide a strategy for new MASLD-related therapies.

4. METHODS

4.1. Animal studies

Floxed matrin-3 mice (Matr3$^{fl/fl}$) were generated using the Easi-CRISPR method developed at the University of Nebraska Medical Center Mouse Genome Engineering Core Facility [83,84]. Two guide RNAs (one each upstream- and downstream- to exon 3 of the matrin-3 gene) were used to excise out a target exon and insert a single-stranded donor DNA containing LoxP sites and short homology arms. The sequences of guide RNAs and long ssDNA donor are in Supplemental Figure S2. The Easi-CRISPR components (two guide RNAs, Cas9 protein and long ssDNA donor) were injected into C57BL6/J strain zygotes, and the founder mice were generated following standard procedures described previously [85]. The founder mice were genotyped using two sets of primers, one each for 5′ and 3′ LoxP sites (Figure S2B) and the germline transmitted F1 mice were bred to establish Matr3$^{fl/fl}$ colony. Matr3$^{fl/fl}$ mice were bred with Albumin-Cre mice (The Jackson Laboratory, #003574) to generate liver-specific matrin-3 knockout mice (Matr3$^{fl/fl}$;Alb-Cre+) that were named as Matr3 LKO mice in this study. Male and female mice were housed on a normal 12/12 light−dark cycle. Mice had ad libitum access to a normal chow diet (Envigo, cat# 2016) and water, or a high-fat diet (HFD) with 60 kcal% fat (Research Diets, D12492). Mice (n = 12 mice per group of each sex) were fed a HFD at 7 weeks of age for 16 weeks. Sixteen weeks post-HFD, mice were fasted for 12 h for euthanasia and tissue collection. Blood was collected through cardiac puncture and supplemented with 4 mM EDTA for plasma. Body and liver weight were recorded. The same anatomic lobe of the liver from each mouse was fixed with 10% neutral buffered formalin (Sigma−Aldrich, HT501128) at 4 °C for 24 h, and other lobes were snap-frozen for storage at −80 °C.

4.2. The administration of CAR agonist TCPOBOP

To activate mouse CAR by its agonist 2,2'-[1,4-phenylenebis(oxy)]bis [3,5-dichloro]-pyridine (TCPOBOP; Enzo, BML-GR245-0025), female Matr3$^{fl/fl}$ mice were injected intraperitoneally with either corn oil (Sigma−Aldrich, C8267) or TCPOBOP at 3 mg/kg [51,54,69,86] dissolved in corn oil. Livers were collected 24 h later. To activate mouse CAR in obese mice, female Matr3$^{fl/fl}$ and Matr3 LKO mice were fed an HFD for 16 weeks. In Week 5 of HFD, mice were weekly treated with TCPOBOP (0.5 mg/kg *i.p.*) for 12 weeks [25,87].

4.3. AAV production, amplification, and purification

The following plasmids were used: pAAV.TBG.PI.eGFP.WPRE.bGH (Addgene, 105535), pAAV2/8 (Addgene, 112864), pX552-GFP (Addgene, 107023), and pHelper vector from the AAVpro Helper Free System (Takara, 6673). The mouse CAR gene (*NR1I3*) was synthesized by ThermoFisher Scientific and cloned into a pX552-GFP vector between BsrGI (NEB, R3575) and EcoRI (NEB, R3101S) restriction enzyme sites. Two glycine codons were added between the *GFP* and *NR1I3* genes. The fusion gene was amplified by the primers with restriction site NotI in forward primer and BamHI in reverse primer using Platinum Taq DNA Polymerase High Fidelity (Invitrogen, 11304011), then the PCR product was digested with restriction enzyme NotI (NEB, R3189S) and BamHI (NEB, R3136S), and inserted into pAAV.TBG.PI.eGFP.WPRE.bGH to replace the sequence between these two sites. The resulting plasmid was named pAAV-TBG-GFP-mCAR. To produce recombinant adeno-associated viruses, the AAVpro 293T cell line (Takara, 632273) is used. Briefly, AAVpro 293T cells were cultured in 20 T175 flasks. Cells were transfected with 20 μg pAAV-TBG-GFP-mCAR, 21.9 μg pAAV2/8, and 34.8 μg pHelper (1:1:1 molar ratio) per T175 flask when cells were 90% confluent. Polyethylenimine (PEI) (Polysciences, 23966-1) was used for transfection with a 3:1 ratio of PEI to plasmid DNA (w/w). After 24-hour transfection, media was replaced with 293T culture media supplemented with 2% FBS. After 48 h, the media was collected and fresh media with 2% FBS was added. 48 h later, the media was collected, combined, and spun at 5000 × *g* for 20 min to remove cell debris. Cell pellets were re-suspended in 20 ml AAV freezing buffer (50 mM Tris−HCl pH 7.4, 150 mM sodium chloride, 2 mM magnesium chloride). After three freeze−thaw cycles, cell lysates were clarified by centrifugation at 2500 × *g* for 30 min. Clarified cell lysates and cell culture media were combined, mixed with 25% volume PEG extraction solution [40 % (w/v) PEG-8000, 2.5 M NaCl in sterile water], and incubated on ice for 2 h. The mixture was spun at 2500 × *g* for 30 min at 4 °C. The pellets were dissolved in 6.5 ml AAV freezing medium, treated with 50 units per ml of TurboNuclease (Eton Bioscience, 1400010050) at 37 °C for 1 h. Cesium chloride (CsCl) gradient centrifugation was performed to purify the virus as previously described [88] with minor modifications. Briefly, the nuclease-treated mixture (6.5 ml) was overlaid onto a CsCl solution prepared by dispensing 2.5 ml 1.5 g/ml CsCl below 2.5 ml 1.3 g/ml CsCl in a standard ultraclear tube (Beckman, 344059) and centrifuged at 29,028 RPM (104,000 × *g*) in an SW41 Ti rotor. After centrifugation, fractions containing virus particles were collected and dialyzed in Slide-A-Lyzer Dialysis Cassettes (Thermo Scientific, 66330) at 4 °C for at least 12 h with three buffer (1 × dPBS) exchanges. The virus solution was then concentrated with an Amicon Ultra-4 Centrifugal Filter Unit (Millipore, UFC810024). Viral titer was determined by qPCR according to the protocol "AAV Titration by qPCR Using SYBR Green Technology" from Addgene. Primer sequences are listed in Supplementary Table 1.

4.4. AAV intravenous injection

To express GFP-CAR in mouse liver, Matr3$^{fl/fl}$ and Matr3 LKO mice were fed HFD for 16 weeks. In week 1 or week 9 on HFD, mice were intravenously injected with 1 × 10^{11} genome copies/mouse of AAV8-TBG-GFP or AAV8-TBG-GFP-CAR via tail vein. Mice were euthanized for blood and tissue collection after 16 weeks of HFD.

4.5. Bulk RNA sequencing and analysis

About 100 mg of each liver was snap frozen in liquid nitrogen and used to extract total RNAs with TRIzol reagent. For HFD-fed mice, RNAs were isolated from each of the eight livers for the construction of eight RNA-seq libraries (four for each mouse group). For chow-diet-fed mice, RNAs were isolated from each of eight livers for the construction of four RNA-seq libraries (two for each mouse group); each sequencing library was constructed from a pool of RNAs from two individual livers. Library

construction, RNA sequencing, and differential expression were done by Novogene. Total RNA quality was examined using an Agilent 2100 Bioanalyzer. The RNA Integrity Number of each RNA sample is above 8.5. A total amount of 1 μg RNA per sample was used for library construction. Libraries were generated using NEBNext® Ultra™ RNA Library Prep Kit for Illumina® (NEB, USA) following the manufacturer's recommendations. After clustering, the libraries were sequenced on an Illumina platform and paired-end reads were generated. Raw reads were processed to generate FASTQ format. Reads with high quality were mapped to the mouse reference genome using the STAR software. FeatureCounts was used to count the read numbers mapped to each gene. Differential expression analysis was performed using the DESeq2 R package between Matr3$^{fl/fl}$ and Matr3 LKO groups with two or four biological replicates per group.

4.6. Gene set enrichment analysis

Gene Ontology (GO) enrichment analyses and Kyoto Encyclopedia of Genes and Genomes (KEGG) pathway enrichment analyses were performed on the lists of genes using the Gene Set Enrichment Analysis (GSEA) software (GSEA v4.2.3 for Windows) (https://doi.org/10.1073/pnas.050658010; https://doi.org/10.1038/ng1180). The reference gene sets are "c2.cp.kegg.v7.5.1.symbols.gmt" in the Molecular Signatures Database (MSigDB v7.5.1) and "c5.go.bp.v2023.2.symbols.gmt" in the Molecular Signatures Database (Mouse MSigDB v2023.2.Mm). Ingenuity Pathway Analysis was performed by the Bioinformatics and Systems Biology Core at the University of Nebraska Medical Center. Packages pheatmap (version 1.0.12) and ggplot2 (version 3.3.5) were used to plot heatmaps and GO plots in R (version 4.1.2).

4.7. Publicly available GEO datasets from published studies

Gene read counts of RNA-seq data (gene_reads_2017-06-05_v8_liver.gct) were downloaded from the Genotype-Tissue Expression (GTEx) project (GTEx analysis V8). Gene expression data in the livers of individuals with BMI <30 were used. There are 53 females and 114 males. GEO dataset GSE167523 contains transcriptomic profiles of 98 liver biopsies of NAFLD patients [89]. Among them, 34 are females and 64 are males. Gene expression of matrin-3 (Matr3) and Car (Nr1i3) was normalized by Gapdh. The correlation plots were generated using ggplot2 in R, and the Pearson correlation coefficient (r) was calculated. GEO dataset GSE182668 contains bulk RNA-seq data from the livers of C57BL/6J mice fed a chow diet or a HFD [90]. GEO dataset GSE112199 contains CAR ChIP-seq data from the livers of mice treated with or without CAR agonist [54]. Changes in chromatin accessibility in mouse liver following TCPOBOP exposure [69] were analyzed from dataset GSE104061 downloaded from the GEO.

4.8. Manually curated list of mouse CAR target genes

We manually curated a list of 1779 CAR target genes compiled from three studies (27, 32, 33). In study 1 (27), mice were treated with mouse CAR agonist TCPOBOP (3 mg/kg, i.p.) or corn oil once daily for 4 days. Liver tissues were collected 24 h after the last injection. Genes with q-Value <0.05 and absolute fold change ≥ 1.5 were selected as differentially expressed genes (DEGs). In study 2 (33), mice with treated with TCPOBOP or corn oil as described in study 1. Raw sequencing reads were downloaded from the Gene Expression Omnibus (GSE98666), aligned to the mouse reference genome (GRCm39, annotation GENCODE m27) via STAR (66), quantified with featureCounts (67), and analyzed for differentially expressed genes with DeSeq2 (68). Genes with padj <0.05 and absolute fold change ≥ 1.5 were selected as DEGs. In study 3 (32), mice were treated with TCPOBOP (3 mg/kg) in corn oil by gavage for 3, 6, 12, 18, and 24 h. Genes with FDR <0.05 were selected as DEGs. Genes that are induced or decreased in at least two studies were selected as mouse CAR target genes.

4.9. Bulk ATAC-seq and analysis

Liver tissues were snap-frozen in liquid nitrogen. Eight or six individual livers from HFD-fed or chow-diet-fed mice were used for nuclei isolation as previously described [91]. For each sample, 50,000 nuclei were transferred into a new tube and resuspended in 50 μl transposase reaction mix [25 μl 2 × TD buffer, 2.5 μl transposase, 16.5 μl PBS, 0.5 μl 1% digitonin, 0.5 μl 10% Tween-20, 5 μl RNase free water], followed with incubation at 37 °C for 30 min in a water bath by tapping tubes every 5 min. Transposed DNA was purified using DNA Clean & Concentrator-5 Kit (Zymo Research, D4014) and eluted in 11 μl elution buffer. The same amount (ng) of purified transposed DNA was pre-amplified mixing with RNase-free water up to 15 μl, 5 μl i7 indexed primer, 5 μl i5 indexed primer and 25 μl NEBNext High-Fidelity 2X PCR Master Mix (NEB, M0541S) with the following program: 72 °C 5 min, 98 °C 30 s, (98 °C 10 s, 63 °C 30 s, 72 °C 1 min) × 5 cycles. 5 μl of pre-amplified DNA from each sample was used to perform qPCR to determine additional cycles needed for each sample. Continue PCR on the remaining 45 μl of each pre-amplified DNA for the appropriate number of cycles. Size selection was performed for each amplified DNA library using AMPure XP Reagent (Beckman) to remove primer dimers and large >1000 bp DNA fragments. For HFD-fed mice, we generated eight libraries with four per condition; for chow-diet-fed mice, we generated six libraries with three per condition. Library quality control and sequencing were performed by Novogene. Raw FASTQ files were processed to remove ATAC-seq adapter sequences using trim-galore (0.6.7). Trimmed FASTQ files were aligned to the mouse reference genome mm10 using Bowtie2 (2.4.2). Mitochondrial reads were removed using the command "samtools view -h filename.sorted.bam | grep -v chrM | samtools view -b -h -f 0x2 - |". Picard MarkDuplicates was used to remove PCR duplicates. Peak calling using MACS2 (2.2.7.1) was performed as described in the PEPATAC pipeline [92] with the following settings as default: –shift -75 –extsize 150 –nomodel –call-summits –nolambda –keep-dup all -p 0.05. The "Bedtools intersect -v —a" command was used to remove mm10 ENCODE blacklist regions. To merge peaks from different replicates, we took the iterative overlap peak merging approach described in the PEPATAC pipeline [92]. For differential peak analysis, we used the bedtools multicov to prepare the counts of reads for each replicate within the merged peakset. Differential peaks were identified using the DEseq2 package (4.2.0). Peak annotation was performed with HOMER (4.11) [93] or ChIPseeker (4.1.1) [94]. To produce heatmaps of differential peaks, Bam files were merged and converted to normalized bigwig files using the samtools package and bamCoverage command. The ComputerMatrix tool was used to generate data matrixes of read counts over the overlap peak regions, and the plotHeatmap function was used to generate a heatmap and average plot from the data matrix. Enrichr or Metascape was used for functional analysis of genes that are associated with differential peaks. Changes in chromatin accessibility in mouse liver following TCPOBOP exposure [69] were analyzed from dataset GSE104061 downloaded from the GEO. Data were analyzed as described above in bulk ATAC-seq.

4.10. Histological analyses

The same anatomic lobe of the liver from each mouse was fixed with 10% neutral buffered formalin at 4 °C for 24 h. Fixed liver tissues were embedded in either paraffin or O.C.T. compound (Fisher Scientific, 4585). Paraffin embedding was completed by the Tissue Sciences

Facility at the University of Nebraska Medical Center. Paraffin sections (6 μm thick) were used for Hematoxylin and Eosin (H&E) staining. Images were acquired using ScanScope CS (Aperio Technologies). Lipid areas seen as cytoplasmic vacuoles were quantified using ImageJ. Histological features were used to differentiate a steatotic vacuole from other non-steatotic holes such as bile duct lumens, sinusoidal spaces, vascular spaces, and artefactual clefts [95]. For cryostat sectioning, liver tissues were soaked in 1 × dPBS containing 30% sucrose at 4 °C for at least two days or until the tissues sank to the bottom of the tube before they were embedded in the Tissue-Tek O.C.T. compound. A Leica CM1900 Cryostat was used to cut liver-frozen sections at 10 μm. For immunofluorescence staining with frozen sections, slides with mounted tissue sections were immersed in a 1:1 solution of acetone:methanol mixture at 4 °C for 10 min and then washed with 1 × dPBS containing 0.3% Triton X-100 (PBST) three times with 5 min for each. The sections were then blocked with 0.3% PBST containing 5% goat serum and 1% BSA for 1 h at room temperature and incubated with primary antibodies in the blocking solution for overnight staining at 4 °C. Anti-MPO (Abcam, ab9535), anti-GFP (Abcam, ab290), or anti-matrin-3 (Bethyl, A300-591A) was used at 1:25, 1:1000, and 1:500 dilution, respectively. Slides were washed three times with 0.3% PBST for 5 min each. Subsequently, the slides were incubated with 1:200 diluted secondary antibodies in the blocking solution containing Hoechst for 1 h at room temperature. After the slides were washed three times with 0.3% PBST, 5 min each, they were mounted with coverslips using Fluoromount-G (Southern biotech, 0100-01) and allowed to dry overnight in the dark at room temperature. For immunofluorescence staining with paraffin sections, slides with mounted tissue sections were first incubated at 60 °C for 1 h. The sections were dewaxed going through xylene 5 min, xylene 5 min, ethanol 1 min, ethanol 1 min. The slides were washed with distilled water twice, then heated in 1 × antigen unmasking solution (Vector Laboratories, H-3300) at 99 °C for 20 min. The slides were washed again with distilled water twice. The staining was performed with the same procedures for the frozen section without acetone:methanol fixation. Anti-SAA1/2 (Abcam, ab199030) were used at 1:100 dilution. Secondary antibodies were DyLight™ 649 Goat Anti-Rabbit IgG Antibody (H + L) from the Vector Laboratories. Images were captured using a confocal laser scanning microscope (Nikon A1R-Ti2 [inverted]) or a Nikon Ti-2 inverted fluorescence microscope equipped with a digital camera for colorimetric images. Three random fields per tissue sample were captured and the images were analyzed using ImageJ (Fiji) software.

4.11. Oil Red O staining

Liver frozen sections were used for Oil Red O staining. Briefly, frozen sections were dried at room temperature for 30 min and placed in propylene glycol for 2 min followed by preheated Oil Red O in propylene glycol at 60 °C for 6 min. Tissue sections were differentiated in 85% propylene glycol solution for 1 min and stained in Mayer's hematoxylin for 1 min. Slides were mounted with an aqueous mounting medium and coverslips. Images were captured using a Nikon Ti-2 inverted fluorescence microscope equipped with a digital camera for colorimetric images and quantified using ImageJ.

4.12. ChIP-seq analysis and ChIP-qPCR

The dataset containing raw reads of ChIP-seq was downloaded from the NCBI Gene Expression Omnibus database repository (GSE112199) [54]. The dataset was analyzed by the Bioinformatics Core Research Facility at our institute. Briefly, paired-end reads were quality-controlled via TrimGalore (version 0.6.10) [96], removing any read with uncalled nucleotides (–max_n 0) and trimming reads at a phred score of 20 (-q 20). The remaining reads were aligned against the reference mouse genome (GRCm39) via bwa [97] with otherwise default parameters and resulting bam files were sorted on genomic location via samtools (version 1.9) [97]. The software package MACS (version 2.1) [98] was used to call differential peaks between hCAR and Control samples with p-value <0.001. CAR binding sites at the genomic loci of different genes (Ces2a and Il1r1) were visualized with the Integrative Genomics Viewer. The frozen livers from mice (100 mg per mouse) injected with AAV8-TBG-GFP or AAV8-TBG-GFP-CAR were used for nuclei isolation following the Chang Lab protocol [91]. Isolated nuclei were crosslinked in 200 μl of 1 × PBS containing 1% formaldehyde (Fisher Scientific, BP531-500) at room temperature for 10 min. Cross-linked nuclei were neutralized by the addition of 0.125 M glycine and incubated at room temperature for 5 min. Nuclei were collected by centrifugation at 3500 × *g* for 5 min, the pellet was resuspended in 1 ml CHIP nuclear lysis buffer containing 1% SDS, 10 mM EDTA, 50 mM Tris—HCl (pH 8.1), with protease inhibitor cocktail (Sigma, P8340). The samples were sonicated using a Branson 250 Sonifier Sonicator for seven pulses with each pulse comprising 20 s sonication at 20% power and 1 min rest. Chromatin amount determination and immunoprecipitation were performed as previously described [18]. 10 μg of chromatin, 4 μg antibodies (Purified Rabbit IgG, Bethyl P120-101 or anti-GFP, Abcam ab290), and 20 μl of Dynabeads Protein G (Invitrogen, 10004D) were used for each immunoprecipitation. DNA was eluted and purified using NucleoSpin Gel and PCR Clean-Up kit (Takara, 740609). qPCR was performed with 2 × diluted DNA to check the binding of CAR on promoters of *Ces2a* and *Il1r1*. Primer sequences were listed in Supplementary Table 1.

4.13. Cytoplasmic and nuclear fractionation

Cytoplasmic and nuclear fractionation assay was conducted using the Subcellular Protein Fractionation Kit for Tissues (Thermo Scientific, 87790) following the manufacturer's instructions. Liver tissues (~60 mg) were washed with ice-cold PBS and removed excess liquid on a lab wipe. The tissues were placed in 1.5 ml pre-chilled Eppendorf tubes and cut into small pieces, adding CEB buffer containing protease inhibitor (1 mg tissue with 10 μl buffer). Tissue pieces with buffer were transferred to a pre-chilled Dounce tissue homogenizer and homogenized for 10 strokes with pestle A, and 10 strokes with pestle B. The homogenized tissues were transferred into Pierce Tissue Strainer and placed into a 15 ml conical tube on ice, followed by centrifuge at 500 × *g* for 5 min. The supernatant (cytoplasmic extract) was immediately transferred into a pre-chilled 1.5 ml tube on ice. Ice-cold MEB buffer containing protease inhibitor (1 mg tissue with 6.5 μl buffer) was added to the pellet. The tubes were vortexed for 5 s on the highest setting and incubated at 4 °C for 10 min with gentle mixing. The samples were centrifuged at 3000 × *g* for 5 min. The supernatant (membrane extract) was transferred into a pre-chilled 1.5 ml tube on ice. Finally, the RIPA buffer supplemented with protease inhibitor (1 mg tissue with 2.2 μl buffer) was added to the pellet. The tubes were vortexed on the highest setting for 15 s and incubated at 4 °C for 30 min with gentle mixing. The lysates were centrifuged at 14,000 × *g* for 15 min to collect nuclear extract.

4.14. RNA immunoprecipitation

One hundred mg of the frozen liver was ground to a fine powder in a pre-chilled mortar filled with liquid nitrogen. The tissue powder was transferred into a pre-chilled 10 cm dish on dry ice and exposed to UV light at 400 mJ/cm^2 for cross-linking. Three milliliters of Cross-linking immunoprecipitation lysis buffer containing 50 mM Tris—HCl (pH 7.5),

200 mM NaCl, 1 mM EDTA, 10% glycerol, 01% NP40, 1% Triton X-100, and 0.5% N-lauroylsarcosine supplemented with proteinase inhibitor (Sigma—Aldrich) and RNase inhibitor (Invitrogen, AM2696) was added to resuspend the tissue powder. The lysates were sonicated for 6 pulses with each pulse comprising 5 s sonication at 10% power and 5 s rest. The lysates were transferred to a new tube after centrifugation at 14,000 $\times$ *g* for 10 min at 4 °C. The protein concentration was measured using Pierce BCA Protein Assay Kit (Thermo Scientific, 23225). 500 μl of lysates containing 250 μg of total protein were incubated with antibodies anti-matrin-3 (Bethyl, A300-591A) or purified rabbit IgG conjugated Dynabeads Protein G (Invitrogen) and tumbled at 4 °C overnight. The immuno-complex was washed with 1 ml of ice-cold high stringency, high salt, low salt, and NT2 buffer, 10 min for each with rotation at 4 °C. The washed complex was resuspended in 375 μl PK buffer [100 mM Tris—HCl (pH 7.5), 100 mM NaCl, 1 mM EDTA, 0.2% SDS] with 25 μl of Proteinase K (20 mg/ml) and incubated with rotation at 55 °C for 45 min. RNA was extracted using TRIzol reagent (Thermo Fisher). RNA was converted to cDNA. qPCR was performed to measure the amount of CAR mRNA (Nr1i3) and the results represent the percentage of CAR mRNA in the matrin-3 interacting RNA fraction over that of input.

4.15. Hepatocyte isolation and mRNA stability assay

Mice were euthanized using isoflurane. Each mouse was sprayed with 70% ethanol before the abdominal cavity was opened. To isolate primary mouse hepatocytes, liver perfusion was performed using a 40 ml buffer from GIBCO (#17701-038), and the digestion was performed using 45 ml buffer containing 1 $\times$ HBSS, 5 mM HEPES, 0.5 mM $CaCl_2$, and 22.5 mg collagenase IV. The perfusion buffer and digestion buffer were prewarmed and kept in a 37 °C water bath during perfusion. Live cells were counted by mixing cell suspension 1:1 with Trypan Blue and seeded at 1.2 $\times$ 10^5 cells per well in a collagen-coated 12-well plate. The cells were cultured in William's E medium containing 5% FBS, 0.1 μg/ml glucagon, 10 μg/ml insulin, 0.7 μg/ml dexamethasone, 2 mM glutamine, and 1 $\times$ pen strep. The cells were replaced in fresh culture medium after attaching. The cells were transfected with 30 nM negative control gapmeRs (5′A*A*C*A*C*G*T*C*T*A*T*A*C*G*C′3; * indicates phosphorothioate backbone modification) or matrin-3 gapmeRs (5′C*G*A*T*C*A*T*C*A*A*A*A*C*T*A*T′3) from Qiagen using Lipofectamine 2000 Transfection Reagent. Cells were treated with 5 μg/ml Actinomycin D in fresh medium 24 h after transfection. The cells were collected at 0, 2, 6, and 10 h treatment, followed by total RNA extraction and cDNA synthesis for Nr1i3 mRNA analysis. The Nr1i3 mRNA expression at each time point was calculated as a percentage relative to the zero time point.

4.16. Liver triglyceride quantification

Lipids were extracted from liver tissues (~50 mg per mouse) using a Lipid Extraction Kit (BioVision, K216-50) following the manufacturer's instructions or as previously described [99]. The samples were diluted 1:5 in saline for triglyceride measurement. A 1:2 serial dilution of Triglyceride standard (Pointe Scientific, T7531STD, 200 mg/dL) was measured to make a standard curve. Triglycerides of standards and samples were measured using Triglycerides Reagent (Thermo Scientific, TR22421).

4.17. RNA extraction, reverse transcription, and quantitative PCR

Total RNAs were extracted from mouse tissues after homogenization using TRIzol Reagent (Thermo Fisher, 15596026) according to the manufacturer's instructions. One microgram of RNA was converted to cDNAs using the High-Capacity cDNA Reverse Transcription Kit (Thermo Fisher, 4368814). Quantitative PCRs (qPCRs) were conducted in the CFX Connect Real-Time System (BioRad) using 2$\times$ SYBR Green qPCR Master Mix (Bimake, B21203). Data were normalized by the delta—delta Ct method [100]. Primer sequences are listed in Supplementary Table 1.

4.18. Western blot analysis and quantification

Mice livers were homogenized into RIPA buffer (Thermo Scientific, J63306.AP) containing protease inhibitor cocktail (Sigma, P8340) and phosphatase inhibitor cocktail 3 (Sigma, P0044). The same amount of protein per sample was loaded onto a Bio-Rad precast gel. The gels were transferred to PVDF membranes and blocked in 5% nonfat dry milk (Bio-Rad, 1706404) in 1$\times$ TBST (0.05% Tween-20) for 60 min. After blocking, the membranes were incubated with primary antibodies in the blocking buffer with gentle agitation for 12—24 h at 4 °C. The membranes were washed in 1 $\times$ TBST, and incubated with anti-rabbit (Cell Signaling Technology, 7074) or anti-mouse (Cell Signaling Technology, 7076) HRP-conjugated secondary antibodies in the blocking buffer. After washing, the membranes were incubated with either Pierce ECL Western Blotting Substrate (Thermo Scientific, 32109) or Cytiva Amersham ECL Prime Western Blotting Detection Reagent (Cytiva, RPN2236). X-ray films were used to detect chemiluminescent signals. ImageJ (Fiji) software was used to quantify protein bands. Protein Loading controls GAPDH or β-actin was used to normalize the levels of protein of interest.

4.19. ELISA

Plasma IL-6 was measured using a Mouse IL-6 ELISA Kit (RayBiotech, ELM-IL6), and the samples were diluted 1: 6.66 in 1 $\times$ Assay Diluent provided in the kit for the measurement. Liver samples were homogenized in RIPA buffer supplemented with protease inhibitor, lysates were used for IL-1β and IL-6 measurement by using kit ELM-IL1b-CL and ELM-IL6-CL from RayBiotech. All the measurements and calculations were performed according to the manufacturer's instructions.

4.20. Statistics

The Shapiro—Wilk test was used to check normality. For two-group comparisons, we used the two-tailed unpaired Student's t-test for data with normal distribution, and the F-test for equality of variances was used before using the t-test; the nonparametric Mann—Whitney U test was used for data without passing a normality test. For repeated measures, we performed statistical analysis with a two-way repeated measures ANOVA comparing two groups. All data in graphs were presented as mean ± SEM, and a $P < 0.05$ was considered statistically significant ($^*P < 0.05$, $^{**}P < 0.01$, $^{***}P < 0.001$).

STUDY APPROVAL

All mice studies were approved by the University of Nebraska — Lincoln Institutional Animal Care and Use Committee, IACUC protocol #2245 and #2246. Gene and protein expression in human de-identified liver specimens was performed under the Institutional Review Board (IRB) Approval with IRB Number: 20190419315EX.

CREDIT AUTHORSHIP CONTRIBUTION STATEMENT

Xiao Cheng: Writing — review & editing, Investigation, Data curation. **Vijaya Bhaskar Baki:** Formal analysis, Data curation. **Matthew Moran:** Formal analysis, Data curation. **Baolong Liu:** Formal analysis,

Data curation. **Jiujiu Yu:** Supervision, Conceptualization. **Miaoyun Zhao:** Formal analysis, Data curation. **Qingsheng Li:** Supervision, Methodology, Conceptualization. **Jean-Jack Riethoven:** Formal analysis, Data curation. **Channabasavaiah B. Gurumurth:** Resources, Methodology. **Edward N. Harris:** Writing — review & editing, Data curation, Conceptualization. **Xinghui Sun:** Writing — review & editing, Writing — original draft, Project administration, Formal analysis, Data curation, Conceptualization.

ACKNOWLEDGMENTS

This work was also supported by the National Institutes of Health [HL150536 to X.S.], National Institutes of Health Funded COBRE grant 1P20GM104320 [X.S. through the Nebraska Center for the Prevention of Obesity-related Diseases through Dietary Molecules], and the University of Nebraska Collaboration Initiative to X.S. This work was also in part supported by the National Institutes of Health [GM147913 to E.N.H.]. Part of the mouse CAR and ChIP-Seq analysis was completed utilizing the Holland Computing Center of the University of Nebraska, which receives support from the UNL Office of Research and Economic Development, and the Nebraska Research Initiative (NRI). We thank the Single Cell Genomics Core at the University of Nebraska — Lincoln for single-nucleus Multiome library construction and the Lipidomics Shared Resources at the Medical University of South Carolina for lipidomics analysis. We thank Rolen M Quadros (Mouse Genome Engineering Core Facility, University of Nebraska Medical Center) for his help in developing and establishing the matrin3 floxed mouse line. We thank the Bioinformatics and Systems Biology Core at UNMC for providing Ingenuity Pathway Analysis services, which receives support from the Nebraska Research Initiative (NRI) and NIH (2P20GM103427, 5P30CA036727 and 2U54GM115458).

DECLARATION OF COMPETING INTEREST

The authors have declared that no conflict of interest exists.

DATA AVAILABILITY

Data will be made available on request.

APPENDIX A. SUPPLEMENTARY DATA

Supplementary data to this article can be found online at https://doi.org/10.1016/j.molmet.2024.101977.

REFERENCES

[1] Rinella ME, Lazarus JV, Ratziu V, Francque SM, Sanyal AJ, Kanwal F, et al. A multisociety Delphi consensus statement on new fatty liver disease nomenclature. Hepatology 2023;78(6):1966—86.
[2] Estes C, Razavi H, Loomba R, Younossi Z, Sanyal AJ. Modeling the epidemic of nonalcoholic fatty liver disease demonstrates an exponential increase in burden of disease. Hepatology 2018;67(1):123—33.
[3] Keam SJ. Resmetirom: first approval. Drugs 2024;84(6):729—35.
[4] Johnson JO, Pioro EP, Boehringer A, Chia R, Feit H, Renton AE, et al. Mutations in the Matrin 3 gene cause familial amyotrophic lateral sclerosis. Nat Neurosci 2014;17(5):664—6.
[5] Durslewicz J, Klimaszewska-Wisniewska A, Antosik P, Grzanka D. Low expression of MATR3 is associated with poor survival in clear cell renal cell carcinoma. Biomedicines 2023;11(2):326.
[6] Yang WC, Lin SF, Wu SC, Shu CW. Matrin3 (MATR3) expression is associated with hemophagocytosis. Biomedicines 2022;10(9):2161.
[7] Quintero-Rivera F, Xi QJ, Keppler-Noreuil KM, Lee JH, Higgins AW, Anchan RM, et al. MATR3 disruption in human and mouse associated with bicuspid aortic valve, aortic coarctation and patent ductus arteriosus. Hum Mol Genet 2015;24(8):2375—89.
[8] Ngo ST, Steyn FJ. The interplay between metabolic homeostasis and neurodegeneration: insights into the neurometabolic nature of amyotrophic lateral sclerosis. Cell Regen 2015;4(1):5.
[9] Nodera H, Takamatsu N, Muguruma N, Ukimoto K, Nishio S, Oda M, et al. Frequent hepatic steatosis in amyotrophic lateral sclerosis: implication for systemic involvement. Neurol Clin Neurosci 2015;3(2):58—62.
[10] Runfola V, Giambruno R, Caronni C, Pannese M, Andolfo A, Gabellini D. MATR3 is an endogenous inhibitor of DUX4 in FSHD muscular dystrophy. Cell Rep 2023;42(9):113120.
[11] Zhang Y, Cao X, Gao Z, Ma X, Wang Q, Xu X, et al. MATR3-antisense LINE1 RNA meshwork scaffolds higher-order chromatin organization. EMBO Rep 2023;24(8):e57550.
[12] Liu T, Zhu Q, Kai Y, Bingham T, Wang S, Cha HJ, et al. Matrin3 mediates differentiation through stabilizing chromatin loop-domain interactions and YY1 mediated enhancer-promoter interactions. Nat Commun 2024;15(1):1274.
[13] Muys BR, Shrestha RL, Anastasakis DG, Pongor L, Li XL, Grammatikakis I, et al. Matrin3 regulates mitotic spindle dynamics by controlling alternative splicing of CDC14B. Cell Rep 2023;42(3):112260.
[14] Islam Z, Polash A, Suzawa M, Chim B, Kuhn S, Sultana S, et al. MATRIN3 deficiency triggers autoinflammation via cGAS-STING activation. bioRxiv 2024.
[15] Sun Z, Chen W, Wang Z, Wang S, Zan J, Zheng L, et al. Matr3 reshapes m6A modification complex to alleviate macrophage inflammation during atherosclerosis. Clin Immunol 2022;245:109176.
[16] Salton M, Elkon R, Borodina T, Davydov A, Yaspo ML, Halperin E, et al. Matrin 3 binds and stabilizes mRNA. PLoS One 2011;6(8):e23882.
[17] Przygodzka P, Boncela J, Cierniewski CS. Matrin 3 as a key regulator of endothelial cell survival. Exp Cell Res 2011;317(6):802—11.
[18] Shihabudeen Haider Ali MS, Cheng X, Moran M, Haemmig S, Naldrett MJ, Alvarez S, et al. LncRNA Meg3 protects endothelial function by regulating the DNA damage response. Nucleic Acids Res 2019;47(3):1505—22.
[19] Cheng X, Shihabudeen Haider Ali MS, Moran M, Viana MP, Schlichte SL, Zimmerman MC, et al. Long non-coding RNA Meg3 deficiency impairs glucose homeostasis and insulin signaling by inducing cellular senescence of hepatic endothelium in obesity. Redox Biol 2021;40:101863.
[20] Loomba R, Friedman SL, Shulman GI. Mechanisms and disease consequences of nonalcoholic fatty liver disease. Cell 2021;184(10):2537—64.
[21] Wei P, Zhang J, Egan-Hafley M, Liang S, Moore DD. The nuclear receptor CAR mediates specific xenobiotic induction of drug metabolism. Nature 2000;407(6806):920—3.
[22] Xie W, Barwick JL, Simon CM, Pierce AM, Safe S, Blumberg B, et al. Reciprocal activation of xenobiotic response genes by nuclear receptors SXR/PXR and CAR. Genes Dev 2000;14(23):3014—23.
[23] Oliviero F, Lukowicz C, Boussadia B, Forner-Piquer I, Pascussi JM, Marchi N, et al. Constitutive androstane receptor: a peripheral and a neurovascular stress or environmental sensor. Cells 2020;9(11):2426.
[24] Dong B, Saha PK, Huang W, Chen W, Abu-Elheiga LA, Wakil SJ, et al. Activation of nuclear receptor CAR ameliorates diabetes and fatty liver disease. Proc Natl Acad Sci U S A 2009;106(44):18831—6.
[25] Gao J, He J, Zhai Y, Wada T, Xie W. The constitutive androstane receptor is an anti-obesity nuclear receptor that improves insulin sensitivity. J Biol Chem 2009;284(38):25984—92.
[26] Wang P, Shao X, Bao Y, Zhu J, Chen L, Zhang L, et al. Impact of obese levels on the hepatic expression of nuclear receptors and drug-metabolizing enzymes in adult and offspring mice. Acta Pharm Sin B 2020;10(1):171—85.

[27] Li X, Wang Z, Klaunig JE. Modulation of xenobiotic nuclear receptors in high-fat diet induced non-alcoholic fatty liver disease. Toxicology 2018;410:199–213.
[28] Coassolo L, Liu T, Jung Y, Taylor NP, Zhao M, Charville GW, et al. Mapping transcriptional heterogeneity and metabolic networks in fatty livers at single-cell resolution. iScience 2023;26(1):105802.
[29] Lukowicz C, Ellero-Simatos S, Regnier M, Oliviero F, Lasserre F, Polizzi A, et al. Dimorphic metabolic and endocrine disorders in mice lacking the constitutive androstane receptor. Sci Rep 2019;9(1):20169.
[30] Oliviero F, Klement W, Mary L, Dauwe Y, Lippi Y, Naylies C, et al. CAR protects females from diet-induced steatosis and associated metabolic disorders. Cells 2023;12(18):2218.
[31] Gabay C, Kushner I. Acute-phase proteins and other systemic responses to inflammation. N Engl J Med 1999;340(6):448–54.
[32] Bengmark S. Acute and "chronic" phase reaction-a mother of disease. Clin Nutr 2004;23(6):1256–66.
[33] Jiang B, Wang D, Hu Y, Li W, Liu F, Zhu X, et al. Serum amyloid A1 exacerbates hepatic steatosis via TLR4-mediated NF-kappaB signaling pathway. Mol Metab 2022;59:101462.
[34] Zhao L, Gimple RC, Yang Z, Wei Y, Gustafsson JA, Zhou S. Immunoregulatory functions of nuclear receptors: mechanisms and therapeutic implications. Trends Endocrinol Metab 2020;31(2):93–106.
[35] Chen ML, Huang X, Wang H, Hegner C, Liu Y, Shang J, et al. CAR directs T cell adaptation to bile acids in the small intestine. Nature 2021;593(7857):147–51.
[36] Nakayasu H, Berezney R. Nuclear matrins: identification of the major nuclear matrix proteins. Proc Natl Acad Sci U S A 1991;88(22):10312–6.
[37] Park SR, Cho CS, Xi J, Kang HM, Lee JH. Holistic characterization of single-hepatocyte transcriptome responses to high-fat diet. Am J Physiol Endocrinol Metab 2021;320(2):E244–58.
[38] Quinton LJ, Blahna MT, Jones MR, Allen E, Ferrari JD, Hilliard KL, et al. Hepatocyte-specific mutation of both NF-kappaB RelA and STAT3 abrogates the acute phase response in mice. J Clin Invest 2012;122(5):1758–63.
[39] Sander LE, Sackett SD, Dierssen U, Beraza N, Linke RP, Muller M, et al. Hepatic acute-phase proteins control innate immune responses during infection by promoting myeloid-derived suppressor cell function. J Exp Med 2010;207(7):1453–64.
[40] Han H, Cho JW, Lee S, Yun A, Kim H, Bae D, et al. TRRUST v2: an expanded reference database of human and mouse transcriptional regulatory interactions. Nucleic Acids Res 2018;46(D1):D380–6.
[41] Zhou Y, Zhou B, Pache L, Chang M, Khodabakhshi AH, Tanaseichuk O, et al. Metascape provides a biologist-oriented resource for the analysis of systems-level datasets. Nat Commun 2019;10(1):1523.
[42] Cui JY, Klaassen CD. RNA-Seq reveals common and unique PXR- and CAR-target gene signatures in the mouse liver transcriptome. Biochim Biophys Acta 2016;1859(9):1198–217.
[43] Repa JJ, Berge KE, Pomajzl C, Richardson JA, Hobbs H, Mangelsdorf DJ. Regulation of ATP-binding cassette sterol transporters ABCG5 and ABCG8 by the liver X receptors alpha and beta. J Biol Chem 2002;277(21):18793–800.
[44] Huang L, Zhao A, Lew JL, Zhang T, Hrywna Y, Thompson JR, et al. Farnesoid X receptor activates transcription of the phospholipid pump MDR3. J Biol Chem 2003;278(51):51085–90.
[45] Wang YD, Chen WD, Moore DD, Huang W. FXR: a metabolic regulator and cell protector. Cell Res 2008;18(11):1087–95.
[46] Major J, Crotta S, Finsterbusch K, Chakravarty P, Shah K, Frederico B, et al. Endothelial AHR activity prevents lung barrier disruption in viral infection. Nature 2023;621(7980):813–20.
[47] Wiggins BG, Wang YF, Burke A, Grunberg N, Vlachaki Walker JM, Dore M, et al. Endothelial sensing of AHR ligands regulates intestinal homeostasis. Nature 2023;621(7980):821–9.
[48] Barretto SA, Lasserre F, Fougerat A, Smith L, Fougeray T, Lukowicz C, et al. Gene expression profiling reveals that PXR activation inhibits hepatic PPARalpha activity and decreases FGF21 secretion in male C57Bl6/J mice. Int J Mol Sci 2019;20(15):3767.
[49] Bock KW. Aryl hydrocarbon receptor (AHR): from selected human target genes and crosstalk with transcription factors to multiple AHR functions. Biochem Pharmacol 2019;168:65–70.
[50] Tian J, Marino R, Johnson C, Locker J. Binding of drug-activated CAR/Nr1i3 alters metabolic regulation in the liver. iScience 2018;9:209–28.
[51] Cheng SL, Bammler TK, Cui JY. RNA sequencing reveals age and species differences of constitutive androstane receptor-targeted drug-processing genes in the liver. Drug Metab Dispos 2017;45(7):867–82.
[52] Coelho MB, Attig J, Bellora N, Konig J, Hallegger M, Kayikci M, et al. Nuclear matrix protein Matrin3 regulates alternative splicing and forms overlapping regulatory networks with PTB. EMBO J 2015;34(5):653–68.
[53] Uemura Y, Oshima T, Yamamoto M, Reyes CJ, Costa Cruz PH, Shibuya T, et al. Matrin3 binds directly to intronic pyrimidine-rich sequences and controls alternative splicing. Genes Cells 2017;22(9):785–98.
[54] Niu B, Coslo DM, Bataille AR, Albert I, Pugh BF, Omiecinski CJ. In vivo genome-wide binding interactions of mouse and human constitutive androstane receptors reveal novel gene targets. Nucleic Acids Res 2018;46(16):8385–403.
[55] Li H, Chen T, Cottrell J, Wang H. Nuclear translocation of adenoviral-enhanced yellow fluorescent protein-tagged-human constitutive androstane receptor (hCAR): a novel tool for screening hCAR activators in human primary hepatocytes. Drug Metab Dispos 2009;37(5):1098–106.
[56] Sueyoshi T, Li L, Wang H, Moore R, Kodavanti PR, Lehmler HJ, et al. Flame retardant BDE-47 effectively activates nuclear receptor CAR in human primary hepatocytes. Toxicol Sci 2014;137(2):292–302.
[57] Gao J, Yan J, Xu M, Ren S, Xie W. CAR suppresses hepatic gluconeogenesis by facilitating the ubiquitination and degradation of PGC1alpha. Mol Endocrinol 2015;29(11):1558–70.
[58] Kawamoto T, Sueyoshi T, Zelko I, Moore R, Washburn K, Negishi M. Phenobarbital-responsive nuclear translocation of the receptor CAR in induction of the CYP2B gene. Mol Cell Biol 1999;19(9):6318–22.
[59] Osabe M, Negishi M. Active ERK1/2 protein interacts with the phosphorylated nuclear constitutive active/androstane receptor (CAR; NR1I3), repressing dephosphorylation and sequestering CAR in the cytoplasm. J Biol Chem 2011;286(41):35763–9.
[60] Skoda J, Dusek J, Drastik M, Stefela A, Dohnalova K, Chalupsky K, et al. Diazepam promotes translocation of human constitutive androstane receptor (CAR) via direct interaction with the ligand-binding domain. Cells 2020;9(12):2532.
[61] Liu J, Shang X, Huang S, Xu Y, Lu J, Zhang Y, et al. Construction and characterization of CRISPR/Cas9 knockout rat model of carboxylesterase 2a gene. Mol Pharmacol 2021;100(5):480–90.
[62] Li Y, Zalzala M, Jadhav K, Xu Y, Kasumov T, Yin L, et al. Carboxylesterase 2 prevents liver steatosis by modulating lipolysis, endoplasmic reticulum stress, and lipogenesis and is regulated by hepatocyte nuclear factor 4 alpha in mice. Hepatology 2016;63(6):1860–74.
[63] Chalhoub G, Jamnik A, Pajed L, Kolleritsch S, Hois V, Bagaric A, et al. Carboxylesterase 2a deletion provokes hepatic steatosis and insulin resistance in mice involving impaired diacylglycerol and lysophosphatidylcholine catabolism. Mol Metab 2023;72:101725.
[64] Mizgerd JP, Spieker MR, Doerschuk CM. Early response cytokines and innate immunity: essential roles for TNF receptor 1 and type I IL-1 receptor during Escherichia coli pneumonia in mice. J Immunol 2001;166(6):4042–8.
[65] Di L. The impact of carboxylesterases in drug metabolism and pharmacokinetics. Curr Drug Metab 2019;20(2):91–102.
[66] Luis JP, Simoes CJV, Brito RMM. The therapeutic prospects of targeting IL-1R1 for the modulation of neuroinflammation in central nervous system disorders. Int J Mol Sci 2022;23(3):1731.
[67] Chalhoub G, Kolleritsch S, Maresch LK, Taschler U, Pajed L, Tilp A, et al. Carboxylesterase 2 proteins are efficient diglyceride and monoglyceride lipases possibly implicated in metabolic disease. J Lipid Res 2021;62:100075.

[68] Zhang Y, Cheng X, Aleksunes L, Klaassen CD. Transcription factor-mediated regulation of carboxylesterase enzymes in livers of mice. Drug Metab Dispos 2012;40(6):1191–7.
[69] Lodato NJ, Rampersaud A, Waxman DJ. Impact of CAR agonist ligand TCPOBOP on mouse liver chromatin accessibility. Toxicol Sci 2018;164(1):115–28.
[70] Xu RX, Lambert MH, Wisely BB, Warren EN, Weinert EE, Waitt GM, et al. A structural basis for constitutive activity in the human CAR/RXRalpha heterodimer. Mol Cell 2004;16(6):919–28.
[71] Dussault I, Lin M, Hollister K, Fan M, Termini J, Sherman MA, et al. A structural model of the constitutive androstane receptor defines novel interactions that mediate ligand-independent activity. Mol Cell Biol 2002;22(15):5270–80.
[72] Negishi M, Kobayashi K, Sakuma T, Sueyoshi T. Nuclear receptor phosphorylation in xenobiotic signal transduction. J Biol Chem 2020;295(45):15210–25.
[73] Negishi M. Phenobarbital meets phosphorylation of nuclear receptors. Drug Metab Dispos 2017;45(5):532–9.
[74] McMahon M, Ding S, Jimenez LA, Terranova R, Gerard MA, Vitobello A, et al. Constitutive androstane receptor 1 is constitutively bound to chromatin and 'primed' for transactivation in hepatocytes. Mol Pharmacol 2019;95(1):97–105.
[75] Das Pradhan A, Glynn RJ, Fruchart JC, MacFadyen JG, Zaharris ES, Everett BM, et al. Triglyceride lowering with pemafibrate to reduce cardiovascular risk. N Engl J Med 2022;387(21):1923–34.
[76] Puengel T, Liu H, Guillot A, Heymann F, Tacke F, Peiseler M. Nuclear receptors linking metabolism, inflammation, and fibrosis in nonalcoholic fatty liver disease. Int J Mol Sci 2022;23(5):2668.
[77] Goswamy D, Gonzalez X, Labed SA, Irazoqui JE. C. elegans orphan nuclear receptor NHR-42 represses innate immunity and promotes lipid loss downstream of HLH-30/TFEB. Front Immunol 2023;14:1094145.
[78] Sun L, Sun Z, Wang Q, Zhang Y, Jia Z. Role of nuclear receptor PXR in immune cells and inflammatory diseases. Front Immunol 2022;13:969399.
[79] Choi S, Neequaye P, French SW, Gonzalez FJ, Gyamfi MA. Pregnane X receptor promotes ethanol-induced hepatosteatosis in mice. J Biol Chem 2018;293(1):1–17.
[80] Joseph SB, Castrillo A, Laffitte BA, Mangelsdorf DJ, Tontonoz P. Reciprocal regulation of inflammation and lipid metabolism by liver X receptors. Nat Med 2003;9(2):213–9.
[81] Spann NJ, Glass CK. Sterols and oxysterols in immune cell function. Nat Immunol 2013;14(9):893–900.
[82] Kribelbauer JF, Rastogi C, Bussemaker HJ, Mann RS. Low-affinity binding sites and the transcription factor specificity paradox in eukaryotes. Annu Rev Cell Dev Biol 2019;35:357–79.
[83] Quadros RM, Miura H, Harms DW, Akatsuka H, Sato T, Aida T, et al. Easi-CRISPR: a robust method for one-step generation of mice carrying conditional and insertion alleles using long ssDNA donors and CRISPR ribonucleoproteins. Genome Biol 2017;18(1):92.
[84] Miura H, Quadros RM, Gurumurthy CB, Ohtsuka M. Easi-CRISPR for creating knock-in and conditional knockout mouse models using long ssDNA donors. Nat Protoc 2018;13(1):195–215.
[85] Harms DW, Quadros RM, Seruggia D, Ohtsuka M, Takahashi G, Montoliu L, et al. Mouse genome editing using the CRISPR/Cas system. Curr Protoc Hum Genet 2014;83. 15.7.1–15.7.27.
[86] Shizu R, Benoki S, Numakura Y, Kodama S, Miyata M, Yamazoe Y, et al. Xenobiotic-induced hepatocyte proliferation associated with constitutive active/androstane receptor (CAR) or peroxisome proliferator-activated receptor alpha (PPARalpha) is enhanced by pregnane X receptor (PXR) activation in mice. PLoS One 2013;8(4):e61802.
[87] Cai X, Feng Y, Xu M, Yu C, Xie W. Gadd45b is required in part for the anti-obesity effect of constitutive androstane receptor (CAR). Acta Pharm Sin B 2021;11(2):434–41.
[88] Ayuso E, Mingozzi F, Montane J, Leon X, Anguela XM, Haurigot V, et al. High AAV vector purity results in serotype- and tissue-independent enhancement of transduction efficiency. Gene Ther 2010;17(4):503–10.
[89] Kozumi K, Kodama T, Murai H, Sakane S, Govaere O, Cockell S, et al. Transcriptomics identify thrombospondin-2 as a biomarker for NASH and advanced liver fibrosis. Hepatology 2021;74(5):2452–66.
[90] Bachmann AM, Morel JD, El Alam G, Rodriguez-Lopez S, Imamura de Lima T, Goeminne LJE, et al. Genetic background and sex control the outcome of high-fat diet feeding in mice. iScience 2022;25(6):104468.
[91] Corces MR, Trevino AE, Hamilton EG, Greenside PG, Sinnott-Armstrong NA, Vesuna S, et al. An improved ATAC-seq protocol reduces background and enables interrogation of frozen tissues. Nat Methods 2017;14(10):959–62.
[92] Grandi FC, Modi H, Kampman L, Corces MR. Chromatin accessibility profiling by ATAC-seq. Nat Protoc 2022;17(6):1518–52.
[93] Heinz S, Benner C, Spann N, Bertolino E, Lin YC, Laslo P, et al. Simple combinations of lineage-determining transcription factors prime cis-regulatory elements required for macrophage and B cell identities. Mol Cell 2010;38(4):576–89.
[94] Yu G, Wang LG, He QY. ChIPseeker: an R/Bioconductor package for ChIP peak annotation, comparison and visualization. Bioinformatics 2015;31(14):2382–3.
[95] Tero BW, Fortier B, Soucy AN, Paquette G, Liaw L. Quantification of lipid area within thermogenic mouse perivascular adipose tissue using standardized image analysis in FIJI. J Vasc Res 2022;59(1):43–9.
[96] Krueger F, James F, Ewels P, Afyounian E, Weinstein M, Schuster-Boeckler B, et al. FelixKrueger/TrimGalore: v0.6.10 - add default decompression path (0.6.10). Zenodo; 2023.
[97] Li H, Durbin R. Fast and accurate short read alignment with Burrows-Wheeler transform. Bioinformatics 2009;25(14):1754–60.
[98] Zhang Y, Liu T, Meyer CA, Eeckhoute J, Johnson DS, Bernstein BE, et al. Model-based analysis of ChIP-seq (MACS). Genome Biol 2008;9(9):R137.
[99] Gosis BS, Wada S, Thorsheim C, Li K, Jung S, Rhoades JH, et al. Inhibition of nonalcoholic fatty liver disease in mice by selective inhibition of mTORC1. Science 2022;376(6590):eabf8271.
[100] Livak KJ, Schmittgen TD. Analysis of relative gene expression data using real-time quantitative PCR and the 2(-Delta Delta C(T)) method. Methods 2001;25(4):402–8.

